Mon. Not. R. Astron. Soc. **000**, 000–000 (0000) Printed 4 December 2010 (MN LATEX style file v2.2)

Thin, thick and dark discs in ΛCDM

J. I. Read*[1], G. Lake[1], O. Agertz[1] & Victor P. Debattista[2]
[1] *Institute of Theoretical Physics, University of Zürich, Winterthurerstrasse 190, 8057 Zürich, Switzerland.*
[2] *RCUK Fellow; Centre For Astrophysics, University of Central Lancashire, Preston, PR1 2HE, UK.*

4 December 2010

ABSTRACT

In a ΛCDM cosmology, the Milky Way accretes satellites into the stellar disc. We use cosmological simulations to assess the frequency of near disc plane and higher inclination accretion events, and collisionless simulations of satellite mergers to quantify the final state of the accreted material and the effect on the thin disc.

On average, a Milky Way-sized galaxy has 1.5 subhalos with $v_{\rm max} > 80\,{\rm km/s}$; 5 with $v_{\rm max} > 60\,{\rm km/s}$; and 13 with $v_{\rm max} > 40\,{\rm km/s}$ merge at redshift $z \gtrsim 1$. A third of these merge at an impact angle $\theta < 20^{\rm o}$ and are dragged into the disc plane by dynamical friction. Their accreted stars *and dark matter* settle into a thick disc. The stellar thick disc qualitatively reproduces the observed thick disc at the solar neighbourhood, but is less massive by a factor $\sim 2-10$. The dark matter disc contributes $\rho_{\rm DDISC} = 0.25-1\,\rho_{\rm HALO}$ at the solar position. Although not likely to be dynamically interesting, the dark disc has important implications for the direct detection of dark matter because of its low velocity with respect to the Earth.

Higher inclination encounters $\theta > 20^{\rm o}$ are twice as likely as low inclination ones. These lead to structures that closely resemble the inner/outer stellar halos recently discovered by Carollo et al. (2007). They also do more damage to the Milky Way stellar disc creating a more pronounced flare, and warp; both long-lived and consistent with current observations. The most massive mergers ($v_{\rm max} \gtrsim 80\,{\rm km/s}$) heat the thin disc enough to produce a thick disc. These heated thin disc stars are essential for obtaining a thick disc as massive as that seen in the Milky Way; they likely comprise some $\sim 50-90\%$ of the thick disc stars. The Milky Way thin disc must reform from fresh gas after $z = 1$.

Only one in four of our sample Milky Way halos experiences mergers massive and late enough to fully destroy the thin disc. We conclude that thick, thin and dark discs occur naturally within a ΛCDM cosmology.

Key words:

1 INTRODUCTION

The energy density of the Universe is primarily composed of a cosmological constant Λ (72%) and cold dark matter (22%) (ΛCDM; Spergel et al. 2007; Seljak et al. 2006). Cosmological N-body simulations make accurate predictions for the evolution of the dark matter component, finding self similar dark matter halos that merge hierarchically, resulting in a complex phase space distribution criss-crossed by streams (Moore et al. 1999; Vogelsberger et al. 2008).

The Milky Way provides a natural laboratory for testing such predictions. The Milky Way is composed of a stellar disc, an old stellar halo, a central bar/bulge of stars, and a dark matter halo (Freeman & Bland-Hawthorn 2002), as summarised in Table 1. Many of these components separate into finer substructures that are likely evidence of past accretions. The most visible of these are stellar streams: the Sagittarius stream that completes nearly two wraps in the plane perpendicular to the Galactic disc (Ibata et al. 1994; Majewski et al. 2003); the 'Monoceros' ring that surrounds the Galactic disc (Ibata et al. 2003; Conn et al. 2007); and many smaller streams that have recently been found in the Galactic halo (Belokurov et al. 2006).

More subtle accretion signatures may also be found in the Milky Way disc and stellar halo. Carollo et al. (2007) find an inner and outer stellar halo that are kinematically distinct, suggestive of separate accretion events, while Gilmore & Reid (1983) were the first to find that the Milky Way disc separates into thin and thick components. The thick disc is older ($> 8\,{\rm Gyrs}$), hotter ($\sigma_z \sim 42\,{\rm km/s}$), more metal poor ($\langle[{\rm Fe/H}]\rangle \sim -0.6$), and more slowly rotating (by $\sim 40\,{\rm km/s}$) than the thin disc (see Table 1).

* Email: justin@physik.unizh.ch

Its age separation from the thin disc corresponds to redshift $z = 1$ in ΛCDM, which is the epoch when the merger rate is calculated and observed to drop rapidly as the Universe changes from matter to dark energy domination (Dalcanton & Bernstein 2002; Bensby et al. 2007; Gottlöber et al. 2001; Kampczyk et al. 2006). This is certainly indicative of a merger origin for the thick disc, though there may not be any single well-defined formation epoch (Nordström et al. 2004). Finally, the Milky Way thin disc presents evidence for past accretions in its spiral arms, warp, flare and bar (Gerhard 2002) – all of which may be induced by satellite-disc interactions (see e.g. Dubinski et al. 2008; Kazantzidis et al. 2007).

The Milky Way is not alone in these properties. Streams are now being found in extra-galactic systems – most notably our nearest neighbour Andromeda (Ibata et al. 2007; Martinez-Delgado et al. 2008), while thick discs appear to be ubiquitous (Tsikoudi 1977; Burstein 1979; van Dokkum et al. 1994; Matthews 2000; Dalcanton & Bernstein 2002; Pohlen et al. 2004; Ibata et al. (2005); Yoachim & Dalcanton 2005; Yoachim & Dalcanton 2006; Elmegreen & Elmegreen 2006).

In this paper, we study how the Milky Way disc affects the accretion of satellite galaxies in a ΛCDM cosmology, and how these satellites in turn affect the Milky Way disc. The Milky Way disc is the dominant mass component of the Milky Way interior to the solar circle. It is important because dynamical friction against the disc causes satellites to be preferentially dragged into the disc plane (Quinn & Goodman 1986; Quinn et al. 1993). As satellites are torn apart by tidal forces, they deposit both their stars *and their dark matter* into a thick disc (Lake 1989). The latter point is the key new idea presented in this work: a dark matter disc must form in a ΛCDM cosmology and we set out to quantify its mass and kinematic properties. At the same time, satellite accretions leave interesting morphological signatures in the stars and we quantify these too. Low inclination events give an accreted thick disc (Walker et al. 1996; Peñarrubia et al. 2006); high inclination ones contribute to the Milky Way stellar halo (Bullock & Johnston 2005; Gauthier et al. 2006); and both heat and distort the Milky Way thin disc (Quinn & Goodman 1986; Walker et al. 1996; Huang & Carlberg 1997; Sellwood et al. 1998; Velazquez & White 1999; Font et al. 2001; Abadi et al. 2003; Ardi et al. 2003; Benson et al. 2004; Gauthier et al. 2006; Hayashi & Chiba 2006; Kazantzidis et al. 2007; Villalobos & Helmi 2008).

Satellite heating of the thin disc has been a subject of particular interest in many previous papers. Kazantzidis et al. (2007) were the first to be able to heat the thin disc enough to form a thick disc[1]. This is because they measured and used the high-redshift satellite distribution that is both more massive and more destructive (because the orbits are more radial) than the surviving distribution (see also Diemand et al. 2004). Using the redshift zero satellite distribution will not give enough heating to form a thick disc (Font et al. 2001; Dubinski et al. 2008). Here we also calculate and use the high-redshift satellite distribution. We find similarly to Kazantzidis et al. (2007) that only the most massive of these satellites can heat the thin disc enough to form a thick disc. In addition, we consider what happens to the material accreted in such encounters – both the stars and the dark matter, and we quantify the fraction of the thick disc that can be accreted. This is particularly relevant for extra-galactic systems, where one counter-rotating thick disc has been found that cannot have formed from thin disc heating alone (Yoachim & Dalcanton 2005).

Our strategy is to use a cosmological structure formation simulation to determine the frequency of satellite-disc encounters, and collisionless simulations of satellite mergers to quantify the final state of both the accreted material and the stellar disc. We do not model the gaseous component of the disc, since we are primarily interested in collisionless mergers. Models for the Milky Way suggest that stars have continued to form at a constant rate since $z = 1$, yet the surface density of gas likely remained constant with time due to fresh gas inflow (Rocha-Pinto et al. 2000; Naab & Ostriker 2006; Just & Jahreiss 2007). The gas is important because it can cool and re-form a thin disc in the 8 Gyrs between $z = 1$ and the present. But it is also important because, unlike the stellar disc that is continually heated by mergers, the gas disc cools and maintains a low vertical dispersion. This keeps the density in the disc plane high, producing more significant dynamical friction. As a result, our gas free simulations likely under-estimate the effect of disc plane dragging. To compensate for this, we consider a range of disc masses from half of the present Milky Way disc mass up to its present mass. We will study the effect of gaseous Milky Way discs in future work.

A complementary approach is to run full gas-hydrodynamical simulations of the formation of the Milky Way that include cooling, star formation and feedback physics. Such simulations remain a significant challenge both because of the computational cost of including gas physics, but also owing to uncertainties as to which physics is most important (see e.g. Thacker & Couchman 2000; Ricotti et al. 2002; Abadi et al. 2003; Robertson et al. 2004; Ceverino & Klypin 2007; Governato et al. 2007). Despite these difficulties, Abadi et al. (2003) found a thick disc in their simulated Milky Way that formed from a mix of accreted and heated stars, while in a series of papers, Brook et al. (2004), Brook et al. (2005) and Brook et al. (2007) find thick discs form directly from heated gas in their simulations[2]. Our approach is complementary to these studies. Predictions for the evolution of the dark component rely only on getting the gravitational clustering right and are now robust (Heitmann et al. 2007). We combine these with our knowledge of what galaxies look like in the Universe today to largely side-step the unknown physics of galaxy formation.

This paper is organised as follows. In §2 we use a concordance cosmology simulation to assess the frequency of high and low inclination satellite accretions for a typical Milky

[1] In a study concurrent with our own, Villalobos & Helmi (2008) also consider the formation of thick discs from satellite heating and manage to successfully form heated thick discs. Their focus is on finding unique morphological and kinematic signatures of such accretions; ours is on calculating the expected number and mass of mergers in ΛCDM and the effect these have on an average Milky Way galaxy. In this sense our studies are complementary.

[2] Such models have been historically disfavoured because the thick disc appears to have formed over an extended period (Prochaska et al. 2000).

Way galaxy. In §3, we present a suite of collisionless simulations of disc-satellite mergers, where we vary the satellite impact angle, orbit and mass. Finally, in §4 we present our conclusions.

2 COSMOLOGICAL SIMULATIONS: THE LIKELIHOOD OF DISC ENCOUNTERS

In this section we use a cosmological simulation to assess the likelihood of near-disc plane mergers in the Milky Way. Some movies of the simulation and the subhalo orbits can be seen at: `http://justinread.net`.

2.1 Description of the simulation

We use the cosmological ΛCDM simulation already presented in Diemand et al. (2005). The simulation was run using PkdGRAV (Stadel 2001), with cosmological parameters: $(\Omega_{\rm m}, \Omega_\Lambda, \sigma_8, h)$=(0.268,0.732,0.7,0.71), and a box of size $L_{\rm box} = 90$ Mpc, with 300^3 particles. The initial conditions were generated with GRAFIC2 (Bertschinger 2001). From the simulation volume, we extracted four Milky Way sized halos at a mass resolution of $m_p = 5.7 \times 10^5 M_\odot$.

The subhalos inside each 'Milky Way' and at each redshift output were identified using a new and improved *SKID*[3] algorithm (Stadel 2001) that will be presented in a forthcoming paper. *SKID* finds subhalos in a two-stage process. First, all particles are moved towards their local density maximum and grouped. Second, unbound particles are iteratively removed until a bound structure is converged upon. Neither stage assumes any symmetry in the halos, or arbitrary truncation radii; we considered all halos with > 50 particles. We have significantly improved the first stage by improving the density gradients. These were previously calculated using a zero-order accurate Smoothed Particle Hydrodynamics gradient estimator[4]. This led to many spurious identifications that were then unbound – some $\sim 50\%$ of halos initially selected were fully unbound at the end of stage two. With the improved gradients this is now reduced to $\sim 5\%$. The improvement is very important at high redshift when there is significant merger activity. The previous version of *SKID* would break the largest halos up into small pieces, significantly under-estimating their masses.

Once a subhalo was identified, we found its position by centring on it with the 'shrinking sphere' method described in Read et al. (2006a); we used the peak of the rotation curve[5] of all bound particles about its mass centre as a proxy for mass. Each subhalo was then traced backwards in time, its progenitor being the subhalo at the previous redshift that contains the majority of its particles.

We are interested in finding subhalos that merge with the disc at a given redshift. However, standard merger trees will not suffice since these define a merger as being when a subhalo *enters* the main halo. By this definition the LMC has already merged with the Milky Way! Instead, we define a subhalo as merged if it: (i) has less than a tenth of its peak circular speed considered over all times; and (ii) has passed within $r_{\rm merge}$ of the main halo after $z = 4.35$. Our results are not sensitive to changes in the peak circular speed fraction or the redshift cut, but are sensitive to $r_{\rm merge}$, particularly for subhalos with peak circular speeds $v_{\rm max} \lesssim 40\,{\rm km/s}$. For this reason, we present results for a range of $r_{\rm merge} = 25, 50, 75\,{\rm kpc}$.

2.2 The likelihood of disc plane mergers

Figure 1, left panel, shows the cumulative maximum circular speed function of surviving (dashed) and accreted (solid) subhalos for the four Milky Way-sized halos. There is some cosmic variance amongst the halos – in particular halo 1 is distinctly different from the other three. It has two very massive mergers with $v_{\rm max} \sim 90\,{\rm km/s}$ that occur at $z < 1$, the second just 2.5 Gyrs ago. As we will show in section §3, these are very damaging to a disc, while their late accretion leaves little time to rebuild a thin disc. Halo 4 has just one significant merger and is the lowest mass of the four. As such, it seems likely that halos 2 and 3 are most representative of the Milky Way.

Our results for the surviving subhalos agree well with previous studies (Gao et al. 2004; Ludlow et al. 2008) and have cumulative $v_{\rm max}$ functions well fit by their fitting function:

$$N(>v_{\rm max}) = A\left(\frac{v_{\rm max}}{v_{\rm max}^{\rm host}}\right)^{-\alpha} \quad (1)$$

where $v_{\rm max}^{\rm host}$ is the peak circular speed of the host galaxy; $\alpha = 2.559$; and $A = 0.06$. Our accreted subhalos are well fit by a similar function with an exponential cut-off:

$$N(>v_{\rm max}) = A\left(\frac{v_{\rm max}}{v_{\rm max}^{\rm host}\, v_0}\right)^{-\alpha} \exp\left(-\left(\frac{v_{\rm max}}{v_{\rm max}^{\rm host}\, v_0}\right)^{\beta}\right) \quad (2)$$

The fitted values depend on our choice for the subhalos' point of closest approach, $r_{\rm merge}$. Figure 1, shows results for $r_{\rm merge} = 50\,{\rm kpc}$, for which we obtain best fit values: $A = 2.87$, $v_0 = 0.42$, $\alpha = 2.23$, and $\beta = 4.8$. However, decreasing $r_{\rm merge}$ decreases the number of lower mass subhalo mergers. For $r_{\rm merge} = 25\,{\rm kpc}$ we find: $A = 4.7$, $v_0 = 0.38$, $\alpha = 1.6$, and $\beta = 4.1$, while $r_{\rm merge} = 75\,{\rm kpc}$ gives: $A = 2.5$, $v_0 = 0.42$, $\alpha = 2.35$, and $\beta = 5$. We likely over-estimate the pericentres because of our limited number of simulation outputs, and because, if we were to include stars and gas in these simulations, the subhalos would be more resilient to tides (see e.g. Macciò et al. 2006). However, our results are well converged for $v_{\rm max} > 40\,{\rm km/s}$ and $r_{\rm merge} < 75\,{\rm kpc}$. Since it is these most massive halos that are of most interest for either damaging the disc or depositing accreted material, our choice of $r_{\rm merge}$ is not critical. We assume $r_{\rm merge} = 50\,{\rm kpc}$ from here on.

From our above fits, assuming $v_{\rm max}^{\rm host} = 200\,{\rm km/s}$, we find: 1.5 mergers with $v_{\rm max} > 80\,{\rm km/s}$; 5 with $v_{\rm max} > 60\,{\rm km/s}$; and 13 with $v_{\rm max} > 40\,{\rm km/s}$. Nearly all mergers at $v_{\rm max} > 60\,{\rm km/s}$ are complete by, or shortly after, $z \sim 1$ (see the middle panel of Figure 1). Most of the massive accreted subhalos were found to be on highly eccentric orbits, with $e > 0.8$ (see right-most panel of Figure 1). This agrees well with Kazantzidis et al. (2007) and

[3] `http://www-hpcc.astro.washington.edu /tools /skid.html`.

[4] This is also the reason for the poor performance of SPH in the presence of strong density gradients (Agertz et al. 2006).

[5] Also called the 'circular speed curve'.

	M ($10^{10} M_\odot$)	$\rho(R_\odot)$ ($M_\odot pc^{-3}$)	$\Sigma(R_\odot)$ ($M_\odot pc^{-2}$)	$R_{1/2}$ (kpc)	$z_{1/2}$ (kpc)	$(\sigma_R,\sigma_\phi,\sigma_z)$ (km/s)	v_c (km/s)	$\langle$[Fe/H]$\rangle$ dex	T (Gyrs)	Ref
Thin disc	4.8 ± 0.4	0.09	50	4.7 ± 0.5	$0.2; 0.25$	$39,20,20 \pm 4$	220 ± 3	~ 0	$\lesssim 8$	1,3,5,7–9,13
Thick disc	~ 1	0.011	$5 - 16$	5.9 ± 0.8	0.63 ± 0.18	$63,39,39 \pm 4$	180 ± 10	~ -0.6	$\gtrsim 8$	1,3,5–9,11
Bulge	0.8 ± 0.4	–	–	0.8	0.25	$-,-,117 \pm 5$	–	-0.1 ± 0.04	–	3,10
Inner halo	$\} \sim 0.1$	–	–	$10 - 15^*$	$6 - 9$	$-,-,\sim 100$	~ 50	< -1.6	> 10	2,12
Outer halo		–	–	$15 - 20^*$	–	$-,-,\sim 100$	$\sim -40; -70$	< -2.2	> 10	2,12
Dark halo	~ 100	~ 0.01	~ 15	$50 - 70^+$	–	$-,-,-$	–	–	–	3,4

$*$ These numbers are not half mass scale lengths, but rather radii at which the inner and outer halo dominate.
$+$ This is the half mass radius in spherical polar coordinates, $r_{1/2}$.

Table 1. The distinct components of the Milky Way. From left to right the columns give: mass; local volume density; local surface density for $|z| < 1.1$ kpc; half mass scale length and height (see §3.2); R, ϕ, z velocity dispersion; rotation velocity; mean metallicity; mean age; and references. Where two values are given this reflects the fact that parameters often depend on the magnitude cut, or in which direction one looks (see e.g. Karaali et al. 2004; Jurić et al. 2008; Cabrera-Lavers et al. 2007). Similar results have been observed for nearby extra-galactic systems (see text). Data are taken from: 1:Kuijken & Gilmore 1989; 2:Morrison 1993; 3:Dehnen & Binney 1998; 4:Wilkinson & Evans 1999; 5:Ojha 2001; 6:Soubiran et al. 2003; 7:Karaali et al. 2004; 8:Holmberg & Flynn 2004; 9:Jurić et al. 2008; 10:Fulbright et al. 2006; 11:Bensby et al. 2007; 12:Carollo et al. 2007; 13:Seabroke & Gilmore 2007.

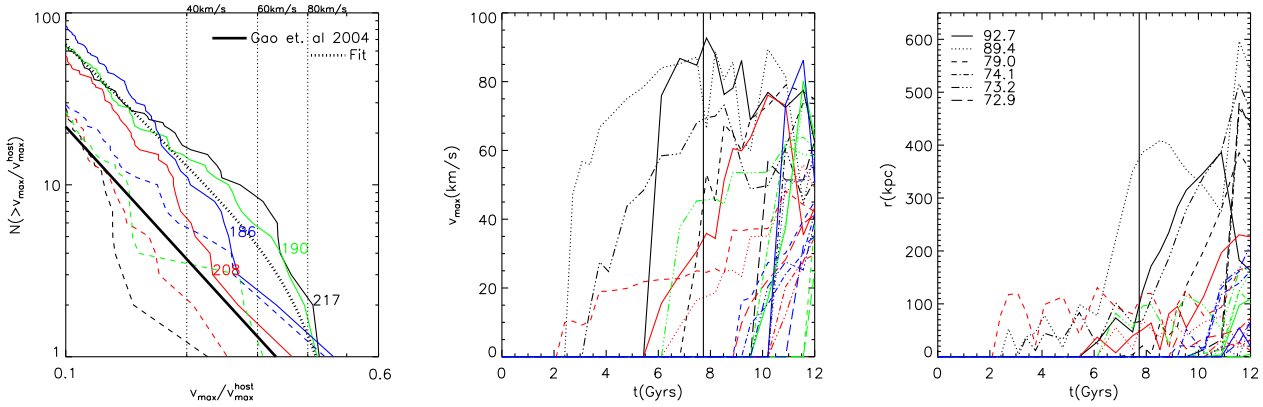

Figure 1. Left: cumulative maximum circular speed $v_{\rm max}$ functions for accreted (solid lines) and surviving (dashed lines) subhalos. We include only halos with greater than 50 particles. For the accreted halos, we consider only halos that at $z = 0$ have 0.1 of their peak $v_{\rm max}$ considered over all times, and which pass within $r_{\rm merge} = 50$ kpc of the disc after $z = 4.35$. Four host halos are shown, taken from the concordance cosmology simulation described in §2 (1 black, 2 red, 3 green, 4 blue); their $v_{\rm max}^{\rm host}$ are marked in km/s. The thick solid line shows a power-law fit to the surviving subhalo $v_{\rm max}$ function taken from Gao et al. (2004) and Ludlow et al. (2008). A fit to the accreted subhalos is also shown (thick dotted line; see text for details). The vertical dotted lines mark $v_{\rm max} = 40, 60, 80$ km/s assuming $v_{\rm max}^{\rm host} = 200$ km/s. **Middle & Right:** evolutionary tracks in $v_{\rm max}$ and radius r for the six most massive subhalos with $v_{\rm max} > 40$ km/s that are accreted by $z = 0$ (solid, dotted, short dashed, dot dashed, triple-dot-dashed and long dashed lines). The different colours correspond to the same four host halos as in the left panel. For halo 1 (black lines) the $v_{\rm max}$ are marked on the right panel in km/s. Redshift $z = 1$ (~ 8 Gyrs) is marked by the vertical solid lines. Note that the pericentres are likely over-estimated due to the limited number of simulation outputs.

Diemand et al. (2004) who find that the accreted subhalos show a more eccentric orbit distribution than the survivors. It is important to stress that the *accreted subhalos are systematically more massive than the survivors*. As pointed out recently by Kazantzidis et al. (2007), it is essential to consider the accreted satellite distribution when studying satellite-disc interactions, otherwise the effects will be underestimated (see also Sales et al. 2007). Here we add the additional point that it is important also to consider only the accreted halos that actually interact with the disc.

Assuming isotropy, the probability that mergers will lie within an angle θ of the disc is given by $P = \sin\theta$. Hence, roughly a third of the mergers will occur with $\theta < 19.5^\circ$, a third with $19.5^\circ < \theta < 41.5^\circ$, and a third with $41.5^\circ < \theta < 90^\circ$. Several recent studies – that focus on the surviving satellites – have found anisotropic satellite distributions, but some find polar alignment (the Holmberg effect; Holmberg 1974; Brainerd 2005; Sales et al. 2007), others find planar alignment (the anti-Holmberg effect; Bailin et al. 2007; Faltenbacher et al. 2007), and some find no statistically significant alignment at all (Azzaro et al. 2006). From our four sample halos, we find two that have a very anisotropic merger history. However, we cannot address the issue directly with our simulations, since we do not know how the disc should align with the halo. In this work we will assume isotropy.

Putting all of the above together, we find that a typical Milky Way sized halo will have 0.5 subhalos merge near the disc plane ($\theta < 20^\circ$) with $v_{\rm max} > 80$ km/s; 1-2 with $v_{\rm max} > 60$; and 4-5 with $v_{\rm max} > 40$ km/s. Away from the disc plane there will be twice as may mergers at the same mass.

Our results agree well with a recent study by Stewart et al. (2007). They use cosmological simulations to study a much larger sample of Milky Way halos than we do (17,000), but at lower resolution. They conclude that 95% of all Milky Way halos have more than one merger with a subhalo $m > 5 \times 10^{10}\,\mathrm{M}_\odot$ ($v_{\rm max} \sim 70\,\mathrm{km/s}$), while 70% have a merger with a subhalo $m > 10^{11}\,\mathrm{M}_\odot$ ($v_{\rm max} \sim 90\,\mathrm{km/s}$). (They define a merger as being anything that enters the virial radius, which corresponds to the sum of our dashed and solid lines in Figure 1, left panel.) They suggest that these latter mergers could prove problematic for thin disc survival. In §3 we will show that such mergers do significantly heat the thin disc, but they do not destroy it; indeed, these mergers (and those at slightly lower mass) are likely to be essential for forming thick discs as massive as that seen in the Milky Way.

As a final point, we remark that it is surprising that subhalos with $v_{\rm max} \sim 60 - 70\,\mathrm{km/s}$ manage to merge in significantly less than a Hubble time. Zhao (2004) showed recently that, once mass loss due to tides is included, dynamical friction times for such subhalos in the Milky Way are greater than 10 Gyrs. Indeed, we will verify that this is the case in §3.3.2 (Gauthier et al. (2006) find similar results in their simulations). Yet such subhalos clearly do merge – and rapidly – in the cosmological simulations. The solution is presented in Figure 2, where we show logarithmic density contours of a spherical region of radius 100 kpc selected around the most massive subhalo in halo 2 at $z = 2.4$. These same particles are tagged and plotted at later times, $z = 1.9$, $z = 1.6$, $z = 1.4$, and $z = 1.2$. Notice that, although this subhalo has $v_{\rm max} = 75\,\mathrm{km/s}$ ($M_{\rm SO} = 2.55 \times 10^{10}\mathrm{M}_\odot$), a much larger region around the subhalo enclosing $10^{11}\,\mathrm{M}_\odot$ (and some other smaller subhalos) largely co-moves with it – subhalos fall in inside larger loosely bound group environments and are effectively deposited at low apocentre. Similar results have been presented recently by Li & Helmi (2007), who suggest that this might explain the apparent alignment of many Local Group galaxies in planes on the sky (see also Lake & D'Onghia 2008 and D'Onghia 2008).

To approximate the effect of the larger group environment, for most of the simulations that follow in §3, we will use a small initial apocentre of $r_a = 30\,\mathrm{kpc}$. We justify this further in §3.3.2 where we show the effect of a larger apocentre orbit[6].

The above is particularly interesting in the context of the Sagittarius dwarf which is currently merging with the Milky Way. Zhao (2004) pointed out that it would have to have been uncomfortably massive in the past in order to arrive at its present location. This tension is resolved once the larger group environment is taken into account. Modelling the effect of this in detail could be essential for a proper understanding of the Sagittarius stream and the orbits of the Large and Small Magellanic Clouds.

[6] Huang & Carlberg (1997) argue, quite reasonably, for starting satellites at larger apocentre since this should be more cosmologically consistent. Here we suggest that it is actually less so because of this larger group environment. Ultimately, the best approach will be to use a full cosmological simulation that self-consistently includes gas physics and star formation.

3 CONTROLLED SIMULATIONS: DRY SATELLITE MERGERS

In §2, we demonstrated that Milky Way sized galaxies will have on average 1-2 satellites merge with $v_{\rm max} > 60\,\mathrm{km/s}$ near the disc plane ($\theta < 20^{\rm o}$) at early times, and twice as many at higher inclinations. In this section, we use a suite of collisionless simulations to measure the morphology and kinematics of the material accreted in such mergers, and the effect on the Milky Way disc. Some movies of our reference simulation LMC-10°can be seen at: `http://justinread.net`.

3.1 Description of the simulations

We set up our Milky Way model (disc+halo system) by adiabatically growing a disc inside a spherical halo. The initial spherical halos were generated from a distribution function using the method described in Kazantzidis et al. (2004) with the added refinement that the halo is composed of two mass species arranged on shells. The outer shell had particles 5× more massive particles than the inner shell, in order to increase the effective resolution in the central parts. We then inserted a massless disc of particles with scale-length, $R_d = 3$ kpc. We slowly grew the mass of this disc over 1.5 Gyr to a final mass of $3 \times 10^{10}\,\mathrm{M}_\odot$ (MW) and $6 \times 10^{10}\,\mathrm{M}_\odot$ (MWB) while holding the disc particles fixed in place. After this time, we set the kinematics of the disc to give a constant Q = 1.5. Evolved in isolation, the MW system formed a small, weak bar after a Hubble time but otherwise did not change significantly; by contrast, the more massive MWB formed a strong bar. Recall that we do not know the total baryonic mass or gas fraction of the Milky Way disc at $z = 1$ when most of these mergers took place, so it is useful to consider a range of disc masses. Our MW model has a peak circular velocity of 220 km/s and the dark matter halo provides 200 km/s of this (see Figure 3). Current mass models for the Milky Way favour lower halo contributions ($\sim 170\,\mathrm{km/s}$; Klypin et al. 2002), so our MW model corresponds to a maximal halo situation; MWB examines the effect of a more dominant disc.

We chose three models for our satellite: Fornax, LMC and LLMC. Fornax, with *dark matter* contribution to the peak circular velocity $v_{\rm max} = 25\,\mathrm{km/s}$, models the satellite on the Fornax dwarf spheroidal galaxy which has a visible mass of $\sim 5 \times 10^7\,\mathrm{M}_\odot$, and a dynamical mass of $M(< 1.5\,\mathrm{kpc}) \sim 7.5 \times 10^8\,\mathrm{M}_\odot$ (Walker et al. 2006). It was initialised as a two component spherical galaxy, with star and dark matter velocities drawn from numerically calculated distribution functions as in Read et al. (2006a). LMC, with $v_{\rm max} = 60\,\mathrm{km/s}$, models the satellite on the Large Magellanic Cloud – the largest surviving satellite of the Milky Way – with visible mass of $M \sim 2.7 \times 10^9\,M_\odot$, and a dynamical mass of $M(< 8.9\,\mathrm{kpc}) = 8.7 \pm 4.3 \times 10^9\,\mathrm{M}_\odot$ (van der Marel et al. 2002). LLMC, with $v_{\rm max} = 80\,\mathrm{km/s}$, is a 'large' LMC model that considers the effect of the most massive mergers found in §2. Both LMC and LLMC were set up as scaled versions of our MW Milky Way model. Our model satellite properties are given in Table 2 and Figure 3. The total peak circular speeds $v^t_{\rm max}$ for Fornax, LMC and LLMC are $v^t_{\rm max} = 30, 70, 90\,\mathrm{km/s}$, respectively. These are all larger than the quoted $v_{\rm max}$ above because those were

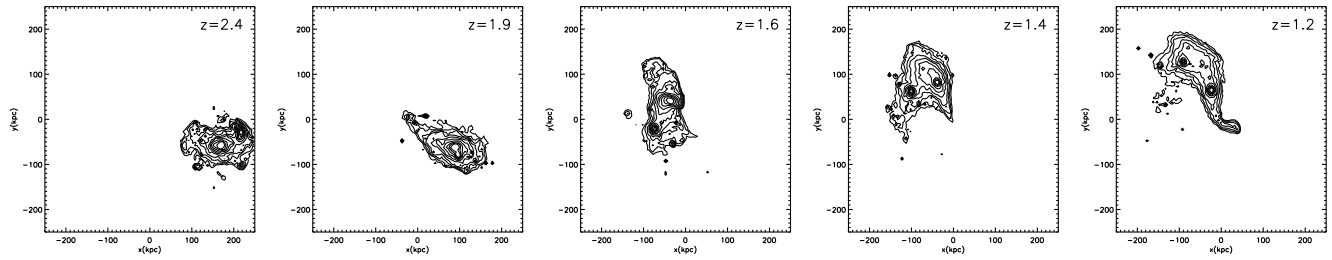

Figure 2. Subhalos fall in inside loosely bound larger groups. Shown here are logarithmic density contours of a spherical region of radius 100 kpc selected around the most massive subhalo in halo 2 at $z = 2.4$, before this subhalo falls into the host halo. These same particles are tagged and plotted at later times, $z = 1.9$, $z = 1.6$, $z = 1.4$, and $z = 1.2$. The peak circular velocity of this subhalo is 75 km/s, while its spherical overdensity mass and radius at $z = 2.4$ are $M_{\rm SO} = 2.55 \times 10^{10} {\rm M}_\odot$ and $r_{\rm SO} = 15.8$ kpc, respectively. The much larger region extending to 100 kpc and enclosing 10^{11} M$_\odot$ (and some other smaller subhalos) largely co-moves with this subhalo.

for only the dark matter contribution to the peak circular speed. We quote $v_{\rm max}$ rather than $v^t_{\rm max}$ from here on for easier comparison with the results from §2.

For the orbit parameters, we chose a wide range of initial inclination angles to the disc from $10 - 60^{\rm o}$, one retrograde orbit (Ret-10$^{\rm o}$), and range of pericentres and apocentres, as detailed in Table 2. We chose a typical apocentre of 30 kpc for reasons outlined in §2. We test the effect of a larger apocentre in one run: LMC-10$^{\rm o}$-abig.

The simulations were evolved using the collisionless tree-code, PkdGRAV (Stadel 2001). We used a maximum timestep of 0.005 Gyrs with nine rungs of decreasing size in powers of two. The final evolved systems were mass and momentum centred using the 'shrinking sphere' method described in Read et al. (2006a), and rotated into their moment of inertia eigenframe with the z axis perpendicular to the disc.

3.2 Some definitions and nomenclature

Some of the density profiles we obtain are not easily fit by a simple functional form. For this reason we use half mass scale lengths[7] as this is then model independent. Discs are typically fit with an exponential profile, given by:

$$\rho(R,z) = \frac{M_0}{4\pi R_0^2 z_0} e^{-R/R_0} e^{-|z|/z_0} \qquad (3)$$

where M_0 is the disc mass, and R_0, z_0 are the scale length and height, respectively. For this distribution, the half mass scale lengths are related to the scale lengths as: $R_{1/2} = 1.68R_0$, $z_{1/2} = 0.7z_0$. Other common variants have $\rho(z) \propto {\rm sech}^2(z/z_s)$ and $\rho(z) \propto e^{-(z/z_e)^2}$, whose scale lengths interrelate as: $z_{1/2} = 0.55z_s = 0.48z_e = 0.7z_0$. We will refer only to the half mass scale lengths from here on.

[7] There can be some confusion here as 'half mass scale length' depends on the choice of coordinates. We work in cylindrical polar coordinates (R, ϕ, z) so that $R_{1/2}$ means the radius containing half of the mass, having already integrated over z and ϕ. Similarly $z_{1/2}$ means the $|z|$ that contains half of the mass, having already integrated over R and ϕ. In spherical polar coordinates (r, θ, ϕ), the half mass radius $r_{1/2}$ is the radius containing half of the mass, having already integrated over θ and ϕ. So $r_{1/2} \neq R_{1/2}$ even in the limit of spherical symmetry.

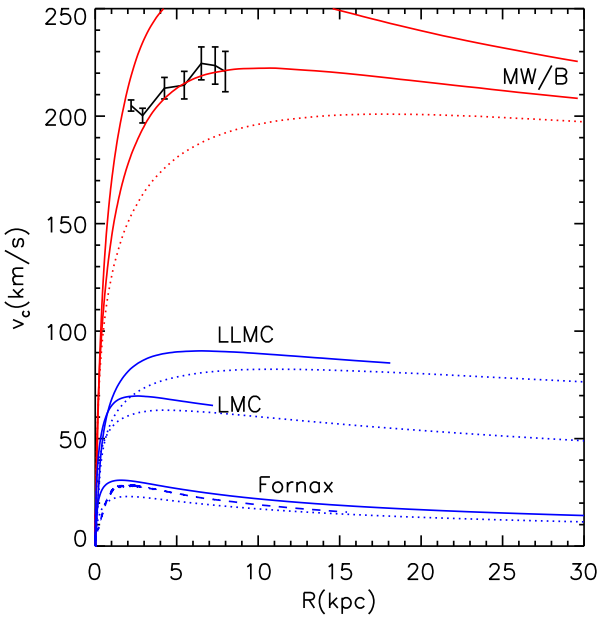

Figure 3. Rotation curves for the different galaxy models. The upper red line is for MWB. The dotted lines show the dark matter halo contribution. The data points show the mean of HI measurements from Bania & Lockman (1984), Weaver & Williams (1974), Weaver & Williams (1973), Malhotra (1995) and Kerr et al. (1986). The blue dashed line shows the rotation curve from one of the subhalos taken from the cosmological simulations of §2.

We also refer frequently to the 'solar neighbourhood'. By this we mean a cylindrical slice centred on $R_\odot = 8.5$ kpc, 1 kpc thick – i.e. $8 < R < 9$ kpc; a slice $7.5 < R < 8.5$ kpc gives nearly indistinguishable results.

3.3 Results

Our main results are shown in Figures 5, 7 and 9. Figure 5 shows the effect of increasing the impact angle; Figure 7, the effect of changing the satellite orbit; and Figure 9, the effect of changing the satellite and host galaxy properties. Some simulations were run for longer to ensure that the final state

Galaxy model	*Description*	N_*	$N_{\rm DM}$	ϵ_*(kpc)	$\epsilon_{\rm DM}$(kpc)	$M_*(\mathrm{M}_\odot)$	r_*(kpc)	$M_{\rm DM}(\mathrm{M}_\odot)$	$r_{\rm DM}$(kpc)
MW	Milky Way; light disc	7.5×10^5	2×10^6	0.06	0.1; 1	3×10^{10}	3	10^{12}	25
MWB	Milky Way	7.5×10^5	2×10^6	0.06	0.1; 1	6×10^{10}	3	10^{12}	25
LLMC	Large-LMC	7.5×10^5	2×10^6	0.015	0.024; 0.234	3×10^9	1.78	1×10^{11}	15
LMC	LMC-like	7.5×10^5	2×10^6	0.015	0.024; 0.234	7×10^8	0.7	2.4×10^{10}	6
Fornax	Fornax-like	10^6	10^6	0.005	0.02	5.6×10^7	0.1	10^9	2

Simulation	(x,y,z) (kpc)	(v_x,v_y,v_z) (km/s)	i	e	*Rotation*	$T_{\rm out}$(Gyrs)
LMC-10°	(29.5,0.27,-5.2)	(-6.3,89.3,0.35)	10°	0.8	*prograde*	6.5
LMC-20°	(28.2,0.12,-10.3)	(-2.2,80.1,0.82)	20°	0.8	*prograde*	4.3
LMC-40°	(23,0.12,-19.3)	(-1.8,80.1,1.52)	40°	0.8	*prograde*	6.3
LMC-60°	(15,0.12,-26)	(-1.2,80.1,2.0)	60°	0.8	*prograde*	7
LMC-Ret-10°	(29.5,0.237,-5.2)	(-6.3,-89.3,0.35)	10°	0.8	*retrograde*	5.3
LMC-10°-eless	(29.5,0.27,-5.2)	(-6.3,143,0.35)	10°	0.36	*prograde*	4.1
LMC-10°-abig	(80,0.27,-15.2)	(-6.3,62.5,0.35)	10°	0.74	*prograde*	6.8
Fornax-10°	(29.5,0.27,-5.2)	(-6.3,89.3,0.35)	10°	0.8	*prograde*	5
LLMC-10°	(29.5,0.27,-5.2)	(-6.3,89.3,0.35)	10°	0.8	*prograde*	5.5
LLMC-10°-MWB	(29.5,0.27,-5.2)	(-6.3,89.3,0.35)	10°	0.8	*prograde*	4.5

Table 2. Simulation labels and parameters. The top table shows the different galaxy models we use, two for the host galaxy (MW/MWB), and three different satellite galaxy models: LMC, LLMC and Fornax. The columns show from left to right: the number of star and dark matter particles, $N_*, N_{\rm DM}$; the force softenings, $\epsilon_*, \epsilon_{\rm DM}$; and the masses and scale lengths of each component, $M_*, r_*, M_{\rm DM}, r_{\rm DM}$. Where two force softenings are given, these are for the low mass inner and higher mass outer halo particles (see §3.1 for details). The bottom table shows the different initial satellite orbits. The columns give from left to right: the initial phase space coordinates of the satellite, x, y, z, v_x, v_y, v_z; the initial inclination to the Milky Way disc, i; the eccentricity, e; the sense of rotation; and the simulation output time.

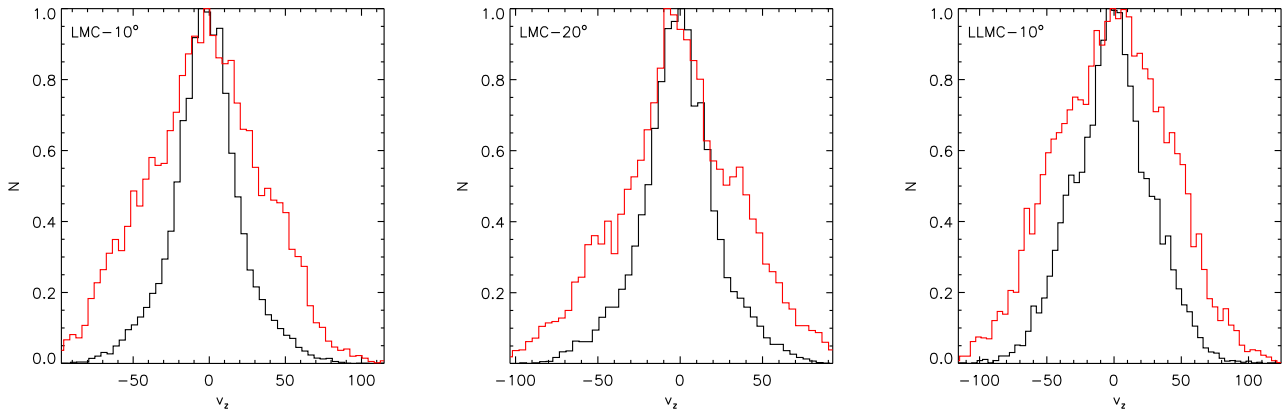

Figure 4. The distribution of v_z velocities at the solar neighbourhood, $8 < R < 9\,$kpc; $|z| < 0.35\,$kpc, for LMC-10°, LMC-20° and LLMC-10°. The black line shows the Milky Way disc stars, the red the accreted satellite material. The distributions are normalised to peak at 1 and do not represent the mass in each component. Notice the prominent wings in the thin disc distribution for LMC-10° and LMC-20°: some of the stars originating in the thin disc show 'thick disc' kinematics. For the more massive LLMC-10°merger, the wings are now very prominent: the heated thin disc distribution looks like the accreted distribution in LMC-10° and little thin disc component remains.

was in equilibrium. Typical times were $\sim 5\,$Gyrs (see Table 2).

Figure 4 shows the distribution of v_z velocities of stars at the solar neighbourhood for LMC-10°, LMC-20° and LLMC-10°. For LMC-10° and LMC-20°, some of the stars originating in the Milky Way thin disc are scattered such that they have thick disc like kinematics (notice the prominent wings), but the majority of stars with thick disc kinematics are accreted. For the more massive satellite merger – LLMC-10° – these wings are now very prominent and little thin disc remains. The heated thin disc distribution now looks like the accreted distribution in LMC-10°.

In most of what follows, we will decompose the final distributions into Milky Way stars and dark matter, and those accreted from the infalling satellite. This decomposition makes sense, since we can expect the accreted satellite stars to be chemically distinct from the thin disc stars. Observations at the solar neighbourhood show that thick and thin disc stars do show different chemistry, while there are some thin disc stars with thick-disc like kinematics (§1 and see Bensby et al. 2007). In §3.3.5, we investigate alternative decompositions where we include heated thin disc stars in the thick disc.

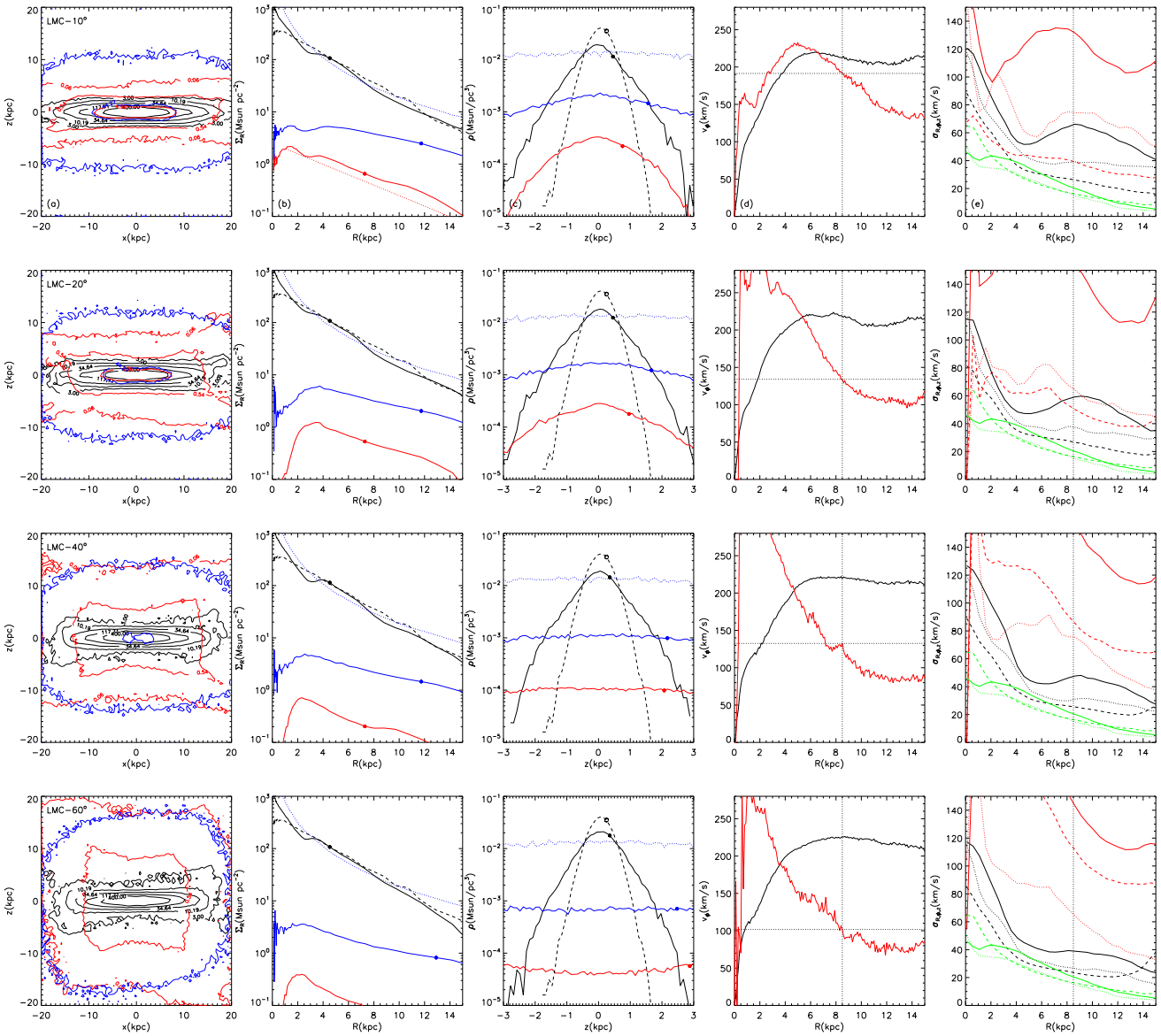

Figure 5. The effect of increasing impact angle: simulations: LMC-10°, LMC-20°, LMC-40° and LMC-60°. From left to right, the panels show: **(a)** logarithmic density contours, viewed from side, in units of $M_\odot\,pc^{-3}$; **(b)** surface density as a function of R in a slice $|z| < 1.1$ kpc (the red dotted line [offset] for simulation LMC-10° shows an exponential fit with scale length $R_0 = R_{1/2}/1.68 = 4.3$ kpc); **(c)** surface density as function of z in a slice $8 < R < 9$ kpc; **(d)** the rotation curve ($v_\phi(R)$ for $|z| < 0.35$ kpc); and **(e)** the R (solid), ϕ (dotted) and z (dashed) components of the stellar velocity dispersion as a function of projected radius. In all cases, we show the Milky Way stars (black), accreted satellite stars (red), Milky Way dark matter (blue dotted) and satellite accreted dark matter (blue). The black dashed lines (left three panels) and green lines (right panel) show the Milky Way disc initial conditions. The solid dots mark the half mass scale lengths for each component. The black dotted lines mark the solar position. Notice that a thick disc of stars forms for impact angles $\lesssim 20°$, with a corresponding thick disc of accreted dark matter. Higher impact angles give more boxy stellar and dark matter distributions that rotate more slowly and are hotter. They also do increasing damage to the Milky Way thin disc, producing a flared outer disc that for LMC-40° and LMC-60° is better described as a warp.

3.3.1 Varying the impact angle

The rows in Figure 5 show the effect of increasing the impact angle: simulations LMC-10°, LMC-20°, LMC-40° and LMC-60°. From left to right, the panels show: (a) logarithmic density contours, viewed from side, in units of $M_\odot\,pc^{-3}$; (b) surface density as a function of R in a slice $|z| < 1.1$ kpc (the red dotted line for simulation LMC-10° shows an exponential fit with scale length $R_0 = R_{1/2}/1.68 = 4.3$ kpc); (c) surface density as function of z in a slice $8 < R < 9$ kpc; (d) the rotation curve ($v_\phi(R)$ for $|z| < 0.35$ kpc); and (e) the R (solid), ϕ (dotted) and z (dashed) components of the stellar velocity dispersion as a function of projected radius. In all cases, we show the Milky Way stars (black), accreted satellite stars (red), Milky Way dark matter (blue dotted) and satellite accreted dark matter (blue). The black dashed

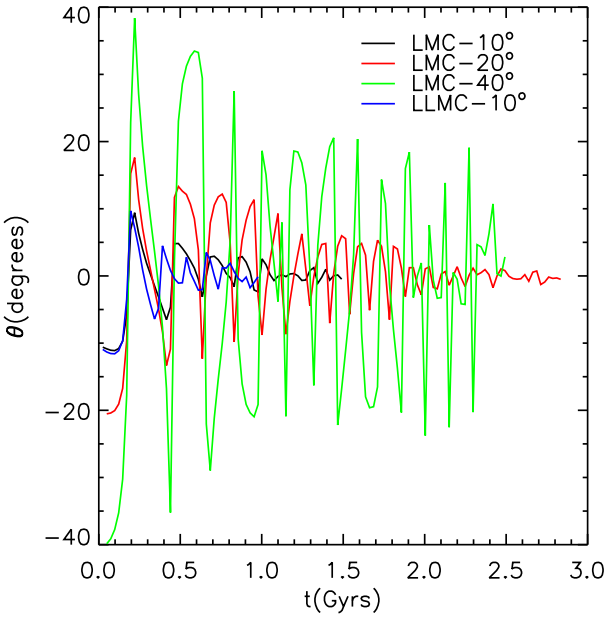

Figure 6. The satellite-disc inclination angle θ as a function of time; lines are truncated when the satellite is fully accreted. For $\theta < 20^{\rm o}$ initially, the satellite is dragged into the disc plane; for $\theta = 40^{\rm o}$ initially, the satellite remains out of the disc plane at all times. Increasing the satellite mass (LLMC-10°) leads to faster disc plane dragging.

lines (left three panels) and green lines (right panel) show the Milky Way disc initial conditions. The solid dots mark the half mass scale lengths for each component.

For $\theta < 20^{\rm o}$ we form a thick disc of stars and dark matter. At the solar neighbourhood ($8 < R < 9\,$kpc) these lag the thin disc rotation (by 20-85 km/s); are hotter ($\sigma_z \sim 40 - 60\,$km/s); and are of longer scale length and larger scale height ($R_{1/2} \sim 7\,$kpc; $z_{1/2} \sim 0.9\,$kpc). The rotational lag of the stellar thick disc and σ_z both increase with the satellite inclination angle, θ. Notice that the thick disc stars lead the rotation towards the Galactic centre. This is because the thick disc distributions have a hole in the centre (see Figure 5(b)). At the solar neighbourhood, a large fraction of thick disc stars are near apocentre and have small tangential velocity. Towards the Galactic centre, this cannot be maintained because of the decreasing density; most thick disc stars at radii $\lesssim 4\,$kpc are near pericentre and have high tangential velocity.

For $\theta > 20^{\rm o}$ we no longer form a thick disc of stars or dark matter. Instead, we have boxy stellar and dark matter distributions that are much hotter ($\sigma_z > 100\,$km/s) and rotate more slowly ($v_c < 100\,$km/s). The boxy stellar material is a strong candidate for the new 'inner halo' structure, recently discovered by Carollo et al. (2007) (see Table 1). A similar retrograde encounter could also explain some of the outer halo. Recall that these high inclination encounters ($\theta > 20^{\rm o}$) are twice as likely as the lower inclination ones (§2).

The movement from disc-like to boxy structures is also clearly seen in Figure 5(c). Notice that for LMC-10°, there is a definite disc in the accreted stars (red line) and dark matter (blue line). For LMC-20°, the discs expand in scale height and length. For LMC-40° and LMC-60°, both distributions are constant in density over the range $-3 < z < 3$ and can no longer be described as discs.

Figure 6 demonstrates that dynamical friction plane dragging is responsible for the formation of accreted thick discs. In all simulations, the inclination angle of the satellite to the disc decreases with time. However, only for $\theta < 20^{\rm o}$ initially, is the satellite completely dragged into the disc plane.

3.3.2 Varying the orbit

Figure 7 investigates the effect of changing the satellite orbit; lines and panels are as in Figure 5. We consider a retrograde encounter with the disc (LMC-Ret-10°); an orbit with low eccentricity (LMC-10°-eless; $e = 0.36$), and an orbit with large apocentre (LMC-10°-abig; $r_a = 81\,$kpc). In the cosmological simulations of §2, we find no strong bias towards prograde or retrograde orbits, suggesting that retrograde mergers should be common (other recent studies also find only weak net rotation for the satellites, see e.g. Sales et al. 2007). From the observational point of view, it is interesting that, of the two extragalactic disc galaxies studied in detail to date, one has a counter-rotating thick disc (Yoachim & Dalcanton 2005). The orbital decay of the satellite for each of these runs and the reference simulation, LMC-10°, are shown in Figure 8.

As compared to the equivalent prograde encounter (LMC-10°), the retrograde satellite disrupts further out leaving a larger hole behind. This can be seen in the radial surface density (Figure 7(b)). This is expected because dynamical friction goes as $1/v^2$. The prograde satellite is nearly stationary with respect to the disc and falls in faster than the retrograde one (Quinn & Goodman 1986). The effect is small, however, because the dark halo dominates the mass as all radii in our MW model (this is not the case for MWB). The larger difference between the prograde and retrograde encounters is in the response of the Milky Way disc; we discuss this in §3.3.4.

The lower eccentricity run, LMC-10°-eless ($e = 0.36$), gives a lower σ_R and a smaller lag in the rotation of the accreted material. The small rotation lag can be increased by increasing the impact angle, θ (see §3.3.1).

The high apocentre run, LMC-10°-abig, is particularly interesting. Even over 7 Gyrs it has not fully accreted and dynamical friction proceeds slowly, despite the satellite being initially of LMC mass. The orbit is shown in Figure 8. The dotted blue line on this plot shows the expected orbit for LMC-10°-abig assuming a static background potential and Chandrasekhar dynamical friction (Binney & Tremaine 2008). The simulated orbit decays much slower because we have not accounted for satellite mass loss due to tides. The satellite, which starts out at $2.4 \times 10^{10}\,{\rm M}_\odot$, is just a few $10^8\,{\rm M}_\odot$ at the end of the simulation. Zhao (2004) have recently highlighted this problem. They show that it is difficult to understand how mergers – like the observed Sagittarius dwarf merger – could proceed in less than a Hubble time without Sagittarius having been unrealistically massive in the past. The solution, as presented in §2, is that most of these galaxies 'ride in' inside larger loosely bound groups

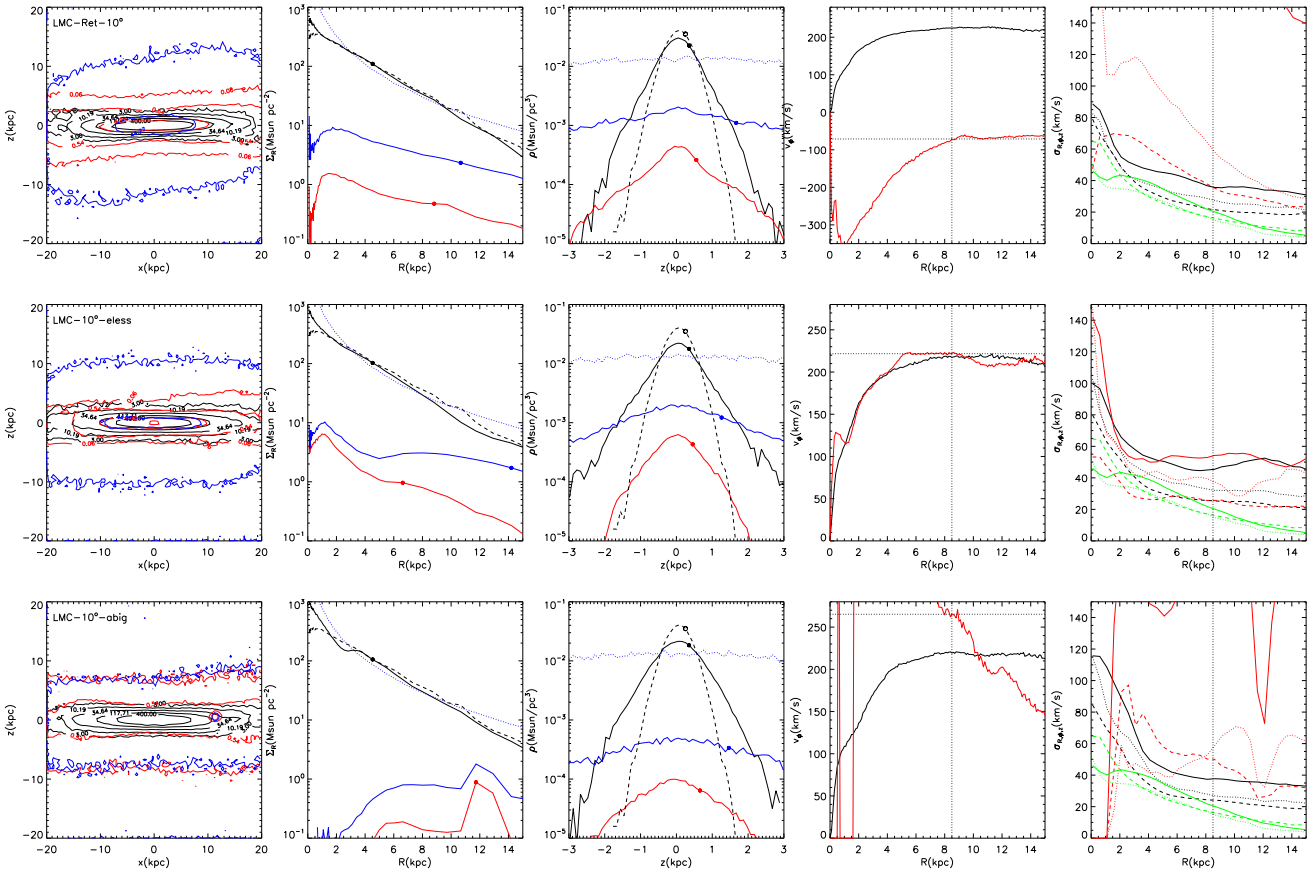

Figure 7. The effect of changing the orbit: simulations: LMC-Ret-10°, LMC-10°-eless and LMC-10°-abig. The lines and panels are as in Figure 5. Notice that the retrograde merger, LMC-Ret-10°, forms a thick disc very similar to the equivalent prograde merger (LMC-10°; Figure 5), though it disrupts further from the centre. It has a quite different effect on the Milky Way disc: a bar does not form, and there is a less pronounced warp/flare. The low eccentricity merger, LMC-10°-eless, produces a higher stellar density at the solar neighbourhood than our reference simulation LMC-10°, but the dark disc density is very similar. The high apocentre merger, LMC-10°-abig, fails to complete merging even over 7 Gyrs (the remnant is visible in the left panel; see also Figure 8) and a significant thick disc is not formed.

and are effectively deposited at low apocentre. This is why our other runs assume $r_a = 30\,\mathrm{kpc}$ for their initial conditions.

3.3.3 Varying the satellite and host galaxy properties

Figure 9 investigates the effect of varying the satellite and host galaxy properties. We consider a low mass satellite (Fornax-10°); a high mass satellite (LLMC-10°); and a more massive Milky Way disc (LLMC-10°-MWB).

The Fornax merger (Fornax-10°) does not produce a structure resembling a thick disc. It disrupts too far out and is destroyed completely by $R \sim 5\,\mathrm{kpc}$. Its rotation velocity leads rather than lags the thin disc (because of the large hole interior to 5 kpc); its dispersions are too high; and the accreted stellar density is two orders of magnitude lower than LMC-10°. Summing over many such mergers could alleviate some of these discrepancies by filling in the hole with accreted material. However, nearly half of such mergers should be retrograde, while from §2, we expect at most ~ 30 such mergers within 20° of the disc plane. The integrated light and dark matter from all such mergers will still be an order of magnitude lower than that contributed by LMC-10°. We conclude that only the most massive mergers are of relevance for contributing accreted stars to the thick disc.

While not forming thick discs, small-satellite encounters do give rise to interesting fine-structure, in this case in the form of a ring[8]. Since the satellite disruption radius will depend more on the satellite mass than on its orbit, ring features could originate from a super-position of satellites. Such super-positions will broaden the ring and make it appear disc-like at large radii. Indeed, this could provide an explanation for the extended disc seen in Andromeda (Ibata et al. 2005 and §1)[9]. From §2, we expect ~ 30 such low inclination, low mass, mergers to occur in the Milky Way. Some of these will have occurred before the disc of the

[8] Rings can also be produced by low density satellites on more circular orbits, though such orbits seem unlikely in our current cosmology (see §2 and Figure 1). High density satellites do not produce rings because they fall in via dynamical friction faster than they disrupt.

[9] Alternative explanations in the literature are to have one large satellite merge in the disc-plane (Peñarrubia et al. 2006); or to have a prograde fly-by from a massive satellite on an eccentric orbit (Younger et al. 2008).

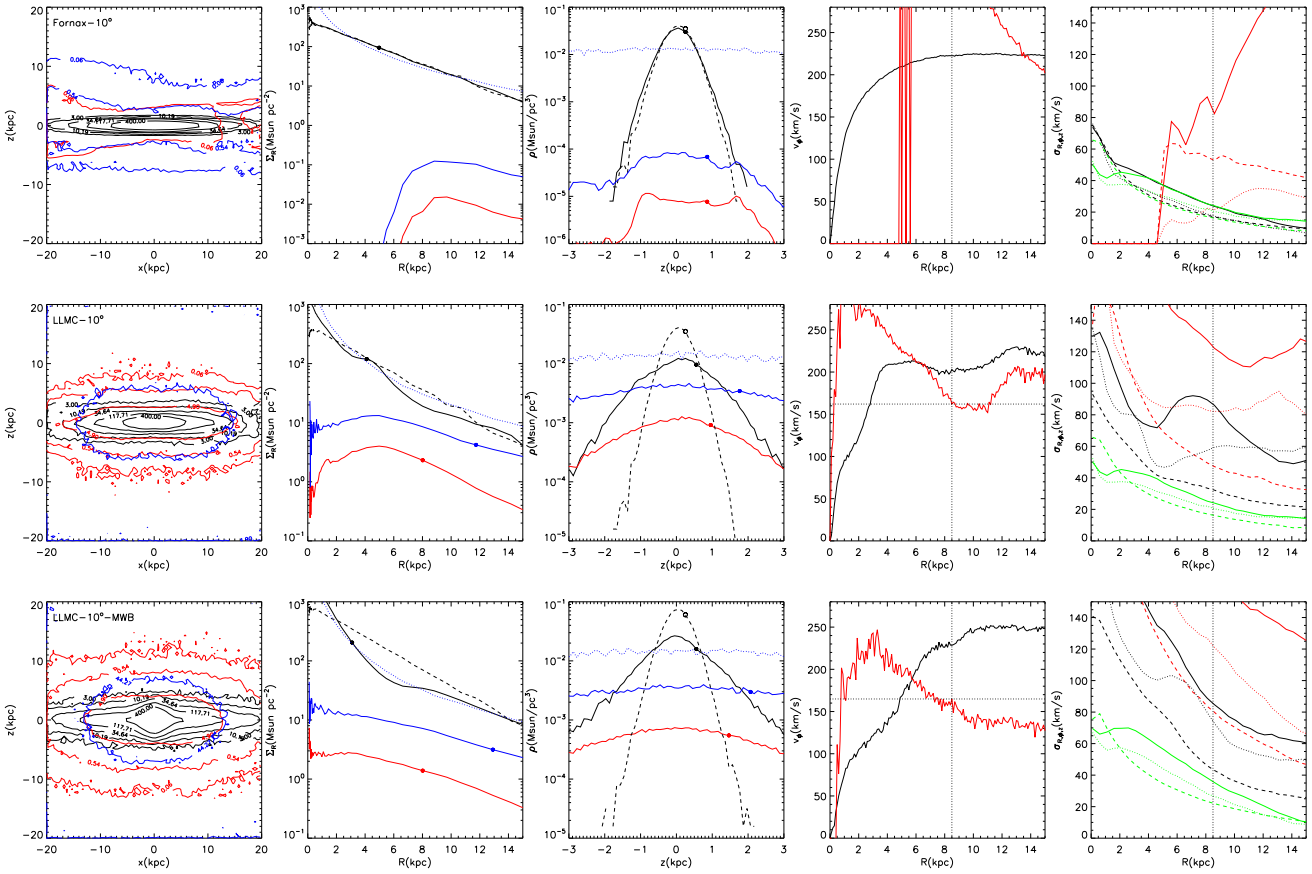

Figure 9. The effect of changing the satellite and host galaxy properties: simulations: Fornax-10°, LLMC-10° and LLMC-10°-MWB. The lines and panels are as in Figure 5. The low mass satellite, Fornax-10°, does not perturb the Milky Way disc at all, nor does it form anything which may be reasonably described as a thick disc. The high mass satellite, LLMC-10° produces results similar to LMC-10°, but does significant damage to the Milky Way disc which now has density comparable to the dark halo at the solar neighbourhood. The more massive Milky Way disc run, LLMC-10°-MWB, produces results similar to LLMC-10°, but the increased disc mass causes a prominent bar to form, while the satellite disrupts more rapidly leading to a thick disc of larger scale height and lower density interior to $|z| < 1.1\,\mathrm{kpc}$.

Milky Way was fully formed and may be essentially undetecable today. However, one such structure does appear to have been observed (Conn et al. 2007). There may be more to be found.

LLMC-10° investigates the effect of increasing the satellite mass. Many of the properties of the accreted material are reminiscent of our reference run – LMC-10°: it lags the rotation of the thin disc by $\sim 40\,\mathrm{km/s}$, is hotter with $\sigma_z \sim 80\,\mathrm{km/s}$ at the solar neighbourhood and is of larger scale height ($z_{1/2} = 0.9\,\mathrm{kpc}$) and longer scale length ($R_{1/2} = 8\,\mathrm{kpc}$) than the thin disc. Such mergers – $v_{\rm max} = 80\,\mathrm{km/s}$ – are not uncommon. Three out of four halos in §2 had a merger more massive than this, while one in three of those will have the merger occur within 20° of the disc plane (assuming isotropy). What is particularly interesting about this simulation, however, is the heating of the thin disc. The final thin disc scale height and kinematics for this run – unlike all of the previous runs – now matches the thick disc of the Milky Way with $z_{1/2} = 0.6\,\mathrm{kpc}$ and $\sigma_z = 40\,\mathrm{kpc}$ at the solar position. We will discuss this in more detail in §3.3.4 and §3.3.5.

Finally, LLMC-10°-MWB investigates the effect of increasing the mass of the Milky Way disc. With the more massive Milky Way disc, the satellite now disrupts further out than in LLMC-10°, leading to a thick disc of larger scale height and lower density interior to $|z| < 1.1\,\mathrm{kpc}$. The more massive disc goes bar unstable without any encounter, forming a prominent bar that appears bulge-like when viewed from the side in projection (a detailed account of this type of instability is given in Debattista et al. 2006).

3.3.4 The Milky Way thin disc: a bar, flare, warp and heated thick disc

Figures 10, 11 and the left-most panels of Figures 5, 7 and 9 show the effect of the mergers on the underlying Milky Way disc. These results should be treated with some caution since we do not know what the Milky Way disc looked like at $z = 1$ and we have assumed near-present day properties for our initial conditions. Nonetheless, the mergers produce a wealth of interesting substructures in the disc that match observations of our own Galaxy, and are long-lived (recall that these simulations have been evolved for $\sim 5\,\mathrm{Gyrs}$ or longer).

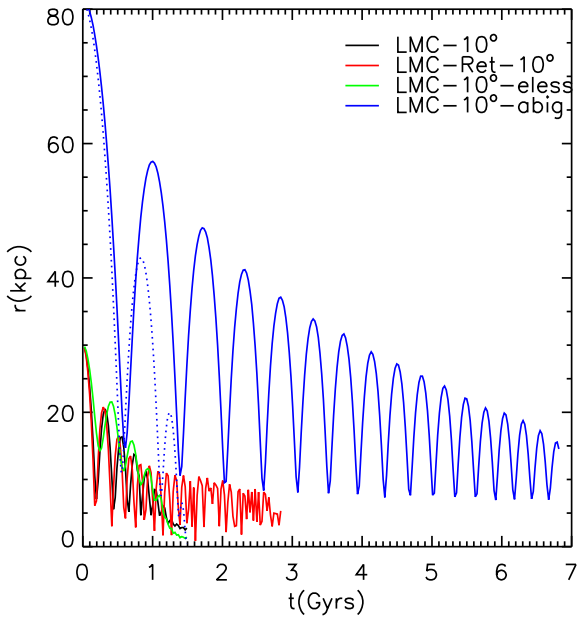

Figure 8. Decay of the satellite orbit as a function of time for selected simulations. The dotted blue line shows the analytic decay rate expected for LMC-10°-abig, assuming Chandrasekhar friction and that the satellite does not lose any mass.

Figure 10 shows the half mass scale height of the Milky Way disc $z_{1/2}$ as a function of R. The different coloured lines show selected simulations; the dashed line shows a fit to data from López-Corredoira et al. (2002) for the Milky Way flare:

$$z_{1/2}(R) = 3.6 \times 10^{-2} R_\odot \exp\left(\frac{R - R_\odot}{12 - 0.6R(\mathrm{kpc})\mathrm{kpc}}\right) \quad (4)$$

with $R_\odot = 7.9\,\mathrm{kpc}$.

The first peak in the distribution is due to the bar, the secondary rise is due to the flared disc. Increasing the impact angle makes very little difference to the size of the bar in scale length or height and in all cases we obtain $z_{1/2} \sim 0.3\,\mathrm{kpc}$; $R \sim 2\,\mathrm{kpc}$. (Changing the satellite orbit also makes almost no discernible difference and we omit these results for clarity.) Increasing the satellite mass increases the bar size by only a modest amount ($R \sim 2.5\,\mathrm{kpc}$). This is interesting because the Milky Way bar appears to be longer than this. López-Corredoira et al. (2007) have recently confirmed the existence of the Milky Way bar using 2MASS star counts. They find dimensions of $3.9 \times 1.2 \times 0.2\,\mathrm{kpc}$. Similarly, Bissantz & Gerhard (2002) have recently found a bar length of 3.5 kpc. The only bar we form that is this long is in LLMC-10°-MWB ($R \sim 4\,\mathrm{kpc}$). This bar forms as a result of secular evolution in the disc and is not driven by the merger. It is also significantly fatter ($z_{1/2} = 0.9\,\mathrm{kpc}$) than the Milky Way bar, though many of these stars would likely be classified as bulge, rather than bar stars[10]. A final interesting point is that the retrograde orbit LMC-Ret-10° hardly excites a bar at all. Such results have been seen in the literature dating back to Holmberg (1941), who presented the first study of prograde versus retrograde interactions. Toomre & Toomre (1972) attribute the phenomenon to increased resonance in the prograde case, but one can also think of it in terms of increased tidal forces for the prograde interaction (see e.g. Read et al. 2006b).

The flare and warp are much stronger indicators of merger activity than the bar. From Figure 10, we can see that the strength of the flare grows with satellite impact angle and is not affected by any other parameter – particularly at large radii ($R > 10\,\mathrm{kpc}$). LMC-60° provides the best match to the observed Milky Way flare. This is encouraging since such mergers should be twice as likely as the low inclination mergers that produce the accreted thick disc.

In Figure 11 we show the mean height of the disc along x' – the direction of maximal height variation; the dashed line shows a fit to data from López-Corredoira et al. (2002) for the Milky Way warp:

$$< z >= 1.2 \times 10^{-6} R(\mathrm{kpc})^{5.25} \sin(\phi + 5^\circ)\mathrm{kpc} \quad (5)$$

We average over $|y'| < 0.5\,\mathrm{kpc}$ and all z. As with the flare, only LMC-60° provides a good match to the observed Milky Way warp.

Levine et al. (2006) have recently suggested that the Milky Way warp is a result of resonant driving by the LMC, but it is intriguing that high impact mergers can produce similar effects, while simultaneously providing a good match to the Milky Way flare. A natural candidate for producing the warp is the Sagittarius dwarf which recently fell in on a polar orbit (Bailin 2003; Bailin & Steinmetz 2005). However, since such merger produced warps are long-lived, earlier mergers could have been more important.

The longevity of the warp is perhaps surprising. Nelson & Tremaine (1995) calculated that dynamical friction ought to rapidly damp such warps away (see also Binney et al. 1998). However, Shen & Sellwood (2006) show that this does not occur in practice because the inner halo moves with the disc. They found, like us, long lived warps that survive over several Gyrs (see also Debattista & Sellwood 1999 and Binney 2007 for a review).

Finally, from Figure 10 notice that the two largest mergers (LLMC-10°and LLMC-10°-MWB; $v_{\max} \sim 80\,\mathrm{km/s}$) heat the thin disc enough that it resembles the thick disc of the Milky Way ($z_{1/2}(R_\odot) \sim 0.6\,\mathrm{kpc}$). None of the lower mass satellites produce enough vertical heating. We discuss the contribution of these heated thin disc stars to the thick disc in §3.3.5.

Our results for the response of the Milky Way disc agree very well with other recent studies in the literature. Dubinski et al. (2008) and Gauthier et al. (2006) merge 100 satellites with a simulated M31 galaxy. They find, like us, a warp, bar and flare that are excited by LMC-mass interactions. Kazantzidis et al. (2007) also find a warp, bar and flare form naturally as a result of disc-satellite interactions in a ΛCDM cosmology. Both of these studies are comple-

[10] The half mass scale height for the Milky Way bulge quoted in Table 1 is 0.25 kpc which seems much smaller than the 0.9 kpc for the secular bugle formed in LLMC-10°-MWB. However, the difference is not so acute. The data for the Milky Way bulge probe only the central $\sim$ 1 kpc, where our secular bulge has a comparable $z_{1/2} \sim 0.3\,\mathrm{kpc}$.

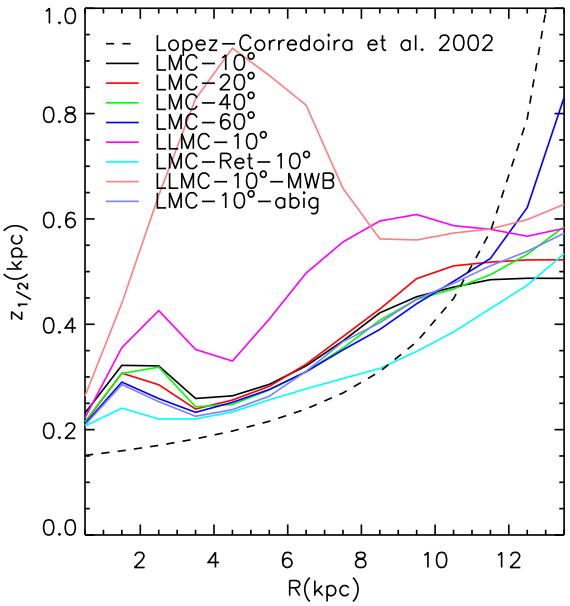

Figure 10. The half mass scale height of the Milky Way disc $z_{1/2}$ as a function of R. The different coloured lines show selected simulations; the dashed line shows a fit to data from López-Corredoira et al. (2002) for the Milky Way flare. The first peak in the simulated distributions is due to the bar, the secondary rise is due to the flared disc.

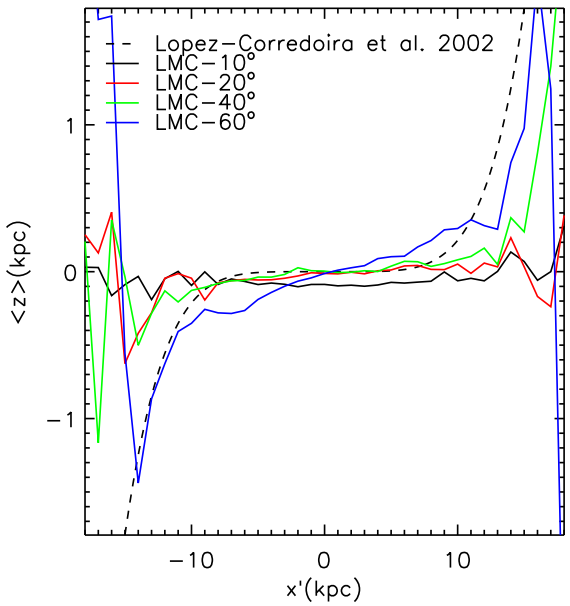

Figure 11. The mean height of the disc along x' – the direction of maximal height variation. We average over $|y'| < 0.5$ kpc and all z. The different coloured lines show selected simulations; the dashed line shows a fit to data from López-Corredoira et al. (2002) for the Milky Way warp.

mentary to ours. Dubinski et al. (2008) and Gauthier et al. (2006) consider the effect of many mergers that occur simultaneously, Kazantzidis et al. (2007) consider the cumulative effect of many interactions that each pass the disc only once, and we follow single interactions over many orbits until they merge. An important difference between Dubinski et al. (2008) and Gauthier et al. (2006) and our study is that they merge the *present surviving* satellite distribution with M31 (this is also the case for most previous studies, e.g. Font et al. 2001). Kazantzidis et al. (2007), like us, use the distribution of accreted satellites that is systematically more massive and more destructive. As a result, these earlier studies underestimate the vertical heating of the disc. A second important difference is that Dubinski et al. (2008) and Gauthier et al. (2006) do not account for the larger group environment around the subhalos. They find that dynamical friction is largely unimportant, as in our LMC-10°-abig simulation. Once the larger group environment is taken into account, dynamical friction does play an important role and allows massive subhalos to successfully merge with the disc at high redshift. Finally our results for retrograde mergers agree well with a study by Velazquez & White (1999). They found, like us, that retrograde interactions give very little disc heating. This demonstrates that the heating is a result of resonant driving from the satellite that is strongly suppressed in retrograde interactions.

3.3.5 Accreted versus heated thick discs

Combining the results from the previous sections, we find that an accreted thick disc of stars forms for impact angles $\lesssim 20^{\rm o}$. For an impact angle of $10^{\rm o} < \theta < 20^{\rm o}$, an eccentricity of $0.36 < e < 0.8$, and a satellite mass of $70 - 90$ km/s, the accreted material has almost all of the observational properties of the Galactic thick disc at the solar neighbourhood ($8 < R < 9$ kpc). For our reference simulation, LMC-10°, we find a thick disc that lags the thin disc rotation by ~ 20km/s, is hotter with $\sigma_z \sim 40$ km/s, compared with $\sigma_z \sim 20$ km/s for the thin disc, and has a larger scale height ($z_{1/2} = 0.7$ kpc) and longer scale length ($R_{1/2} = 7.3$ kpc; $R_0 = 4.3$ kpc) than the thin disc. Increasing θ increases σ_z and the rotation lag; reducing e reduces σ_R and the rotation lag; and increasing the satellite mass increases the velocity dispersion of the thick disc in all directions.

However, as in previous studies (e.g. Walker et al. 1996), our accreted thick discs are significantly less massive than that of the Milky Way. In LMC-10°, we find $\rho_{\rm THICK}/\rho_{\rm THIN} = 0.4\%$ (assuming the *observed value* of $\rho_{\rm THIN} = 0.09\,{\rm M}_\odot\,{\rm pc}^{-3}$), which is too low by a factor ~ 30 (see Table 1). Our other runs produce similar numbers: LLMC-10° gives the most massive thick disc, with $\rho_{\rm THICK}/\rho_{\rm THIN} = 1.3\%$, but even this is too small by a factor ~ 10. In fact, these normalisations are a much closer match to the local $\rho_{\rm HALO}/\rho_{\rm THIN} = 0.5\%$ (Jurić et al. 2008).

The thick disc density normalisation $\rho_{\rm THICK}/\rho_{\rm THIN}$ can be increased by: (i) increasing the satellite stellar mass; (ii) integrating over many near disc plane mergers; and (iii) including heated thin disc stars in the thick disc. A possible fourth mechanism for driving up the mass at the solar position would be to put the stars and dark matter in a ring, rather than a disc. In practice this does not work because dynamical friction drives the satellite inwards as fast as it loses

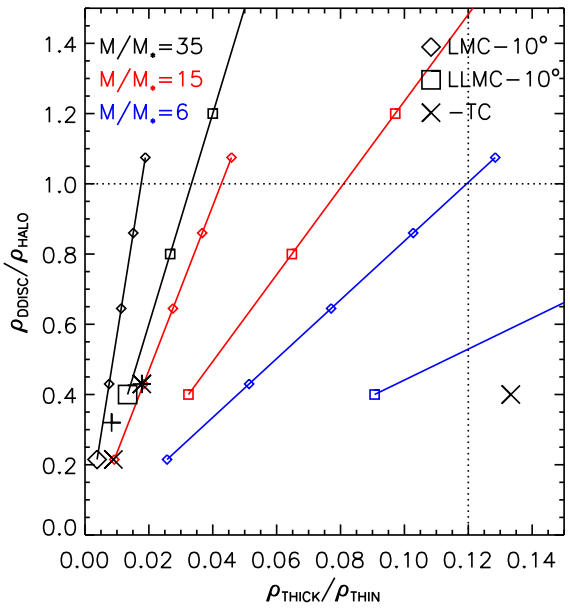

Figure 12. Current constraints on accreted stellar and dark discs at the solar neighbourhood. The plot shows the dark disc to dark halo ratio $\rho_{\rm DDISC}/\rho_{\rm HALO}$ as a function of the thick to thin disc density ratio $\rho_{\rm THICK}/\rho_{\rm THIN}$; we assume for this plot $\rho_{\rm HALO} = 0.01\,{\rm M}_\odot\,{\rm pc}^{-3}$ and $\rho_{\rm THIN} = 0.09\,{\rm M}_\odot\,{\rm pc}^{-3}$. Results are extrapolated from two simulations: LMC-10° and LLMC-10°, marked by the diamond and square, respectively. The star and plus show two additional simulations: LLMC-10°-MWB and LLMCB-10°-MWB, respectively. The different colours extrapolate to lower mass to stellar mass ratio, M/M_*. The solid lines extrapolate to multiple mergers of identical satellites. The X's show the effect of including heated thin disc stars in the thick disc for LMC-10° (60%) and LLMC-10° (90%; see text for details). The vertical dotted black line marks the observed $\rho_{\rm THICK}/\rho_{\rm THIN}$ at the solar neighbourhood.

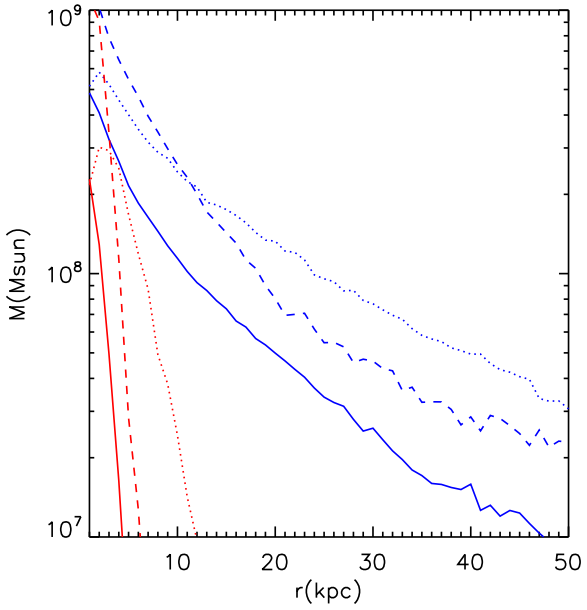

Figure 13. The mass in stars (red) and dark matter (blue) that contribute to the thick discs interior to $|z| < 1.1\,$kpc, as a function of their initial radius within the satellite (in 1 kpc bins) for LMC-10° (solid lines); LLMC-10° (dotted lines); and LLMCB-10°-MWB (dashed lines).

mass and the resulting density at the solar neighbourhood remains low. (We tested this explicitly using test simulations where the satellite was placed on a circular orbit; these are omitted for brevity.)

In Figure 12, we summarise each of the effects (i) to (iii), above by extrapolating the results for LMC-10° and LLMC-10°. Our extrapolations were performed in the following way:

(i) Increasing the satellite stellar mass
We increase the satellite stellar mass while holding the dark matter mass fixed. This is shown by the black red and blue lines in Figure 12 which are for $M/M_* = 35, 15, 6$, respectively.

To test the extrapolation, we ran an additional simulation LLMCB-10°-MWB (shown by the star in Figure 12). This was identical to LLMC-10°-MWB (shown by the plus) except that the satellite had twice the stellar mass. The mass in accreted stars doubled, as expected. However, the mass in the dark disc also increased. The reason for this is given in Figure 13. This shows the mass in stars (red) and dark matter (blue) that contribute to the thick discs interior to $|z| < 1.1\,$kpc, as a function of their initial radius within the satellite for LMC-10° (solid lines); LLMC-10° (dotted lines); and LLMCB-10°-MWB (dashed lines). Most of the mass that contributes originates from the central 10 kpc in the satellite. This is the majority of the stars, but only a fraction of the dark matter. For LLMCB-10°-MWB, the increased disc mass caused the central satellite dark matter to adiabatically contract, causing more dark matter to end up in the thick disc too. This test demonstrates that it is the mass interior to $\sim 10\,$kpc – both stars and dark matter – that contributes to the thick disc. It also explains why the mass to light ratio of our accreted thick discs is lower than that of the satellites from which they form.

(ii) Multiple mergers of like satellites
The solid lines in Figure 12 show the effect of multiple mergers of like satellites. We assume that the accreted material simply adds to that already present. From Figure 1, left panel, we can see that cosmic variance gives an upper bound of ~ 9 mergers above LMC mass. However, for multiple mergers to contribute to the thick disc, they must all be low inclination and prograde. Such a scenario seems unlikely unless accretion occurs along filaments and is highly aniostropic.

(iii) The effect of [heated] thin disc stars
For our most massive mergers – LLMC-10° and LLMC-10°-MWB – the originally thin disc is heated sufficiently that it resembles the Milky Way thick disc at the solar neighbourhood: $\sigma_R \sim 80\,$km/s; $\sigma_\phi \sim 60\,$km/s; $\sigma_z \sim 40\,$km/s; rotation lag $\sim 20\,$km/s; and scale height $z_{1/2} \sim 0.6\,$kpc.

Here we consider the effect of adding these heated thin disc stars to the thick disc, both for the most massive merg-

ers, where almost all of the stars can contribute, and for the less massive merger LMC-10°. We populate the thick disc with thin disc stars at the solar neighbourhood by comparing thick and thin disc distribution functions for each star:

$$f = Ae^{\frac{v_r^2}{2\sigma_r^2}} e^{\frac{(v_\phi - <v_\phi>)^2}{2\sigma_\phi^2}} e^{\frac{v_z^2}{2\sigma_z^2}} e^{\frac{z^2}{z_e^2}} \quad (6)$$

with $\sigma_r = 85\,\mathrm{km/s}$, $\sigma_\phi = 60\,\mathrm{km/s}$, $\sigma_z = 40\,\mathrm{km/s}$, $< v_\phi >= 183\,\mathrm{km/s}$, and $z_e = 1.48\,\mathrm{kpc}$ for the thick disc; and $\sigma_r = 60\,\mathrm{km/s}$, $\sigma_\phi = 40\,\mathrm{km/s}$, $\sigma_z = 19\,\mathrm{km/s}$, $< v_\phi >= 200\,\mathrm{km/s}$, and $z_e = 0.85\,\mathrm{kpc}$ for the thin disc. These choices are motivated by our results in §3.3.1, but our results are not sensitive to these parameters. We assign thin disc stars to the thick disc if $f_{\mathrm{THICK}}/f_{\mathrm{THIN}} > 1$ for that star. We then vary the fraction of thin disc contaminants by varying the relative normalisation of each distribution, A.

For our reference simulation, LMC-10°, we find that we can populate up to 60% of the thick disc with hot thin disc stars without significantly reducing the thick disc scale height. However, greater contamination than this leads to a thick disc that is too cold vertically. For LLMC-10°, the more massive satellite heats the thin disc enough that it resembles a thick disc. A decomposition is still required, however, since the heated thin disc at the end of the simulation does not show enough rotation lag (see Figure 9(d)). We find that for this simulation 90% contamination gives a good qualitative match to the Milky Way thick disc and recovers the full observed thick disc mass. We show the effect of 60% thin disc contamination for LMC-10° and 90% for LLMC-10° by the X's in Figure 12.

From Figure 12, we can see that while multiple mergers and lower M/M_* help to increase the thick disc mass, heated thin disc stars due to a very massive merger ($v_{\mathrm{max}} \sim 80\,\mathrm{km/s}$) seem essential for reaching the high thick disc mass observed in the Milky Way. Accreted stars likely contribute $10 - 50\%$ of the observed thick disc. This is in reasonable agreement with the recent cosmological simulation of Abadi et al. (2003), where they find a thick disc that is equally composed of heated thin disc stars and accreted material. Villalobos & Helmi (2008), also find that accreted stars can make up only a small fraction of the thick disc in the disc plane.

The above seems at odds with the recent extragalactic observations of FGC1415 (Yoachim & Dalcanton 2005), which shows a massive counter-rotating thick disc. A possible solution is that FGC1415 had a rather more massive (and more rare) retrograde merger than those studied here.

In principle, heated and accreted stars should be separable by their chemistry. The high $\rho_{\mathrm{THICK}}/\rho_{\mathrm{THIN}}$ obtained at the solar neighbourhood comes from a fit to star counts for stars that are well separated in colour, but for which there is currently no spectroscopic information (Jurić et al. 2008). But this work will be difficult. State-of-the-art spectroscopic studies have too few stars (~ 200) to obtain an accurate density distribution (Bensby et al. 2007).

As a final note for this section, recall that the Milky Way thick disc has stellar mass $\sim 10^{10}\,\mathrm{M}_\odot$, while the stellar halo is $\sim 10^9\,\mathrm{M}_\odot$ (see Table 1). If we put too many accreted stars into the thick disc then we have a problem: the stellar halo will become too massive because there will be two high inclination mergers for every merger near the disc plane. This suggests that either the Milky Way had its most massive merger near the disc plane, or – which is more likely – a significant fraction of the Milky Way thick disc comprises heated thin disc stars.

3.3.6 A dark matter thick disc

A key new idea presented in this work is that near-disc accretion – that must occur in a ΛCDM cosmology – leads to the formation of a dark matter disc, as well as an accreted stellar thick disc. We can see this in the left three panels of Figure 5 (blue lines). For impact angles $< 20°$, a dark disc forms. For LMC-10° it has scale length and height given by: $R_{1/2} = 11.7\,\mathrm{kpc}$, $z_{1/2} = 1.5\,\mathrm{kpc}$, while its density at the solar neighbourhood is $\rho_{\mathrm{DDISC}}(R_\odot) = 0.22\rho_{\mathrm{HALO}}$ (assuming $\rho_{\mathrm{HALO}} = 0.01\,\mathrm{M}_\odot\,\mathrm{pc}^{-3}$). For LLMC-10° it has $z_{1/2} = 1.7\,\mathrm{kpc}$ and $\rho_{\mathrm{DDISC}}(R_\odot) = 0.42\rho_{\mathrm{HALO}}$. At these low densities, the dark disc is not dynamically interesting in the disc plane. Integrating over the total expected mergers brings the density up, but it is hard for it to exceed the density of the dark halo at the solar neighbourhood without having an unrealistically high number of mergers (see §2). The extrapolated constraints for LMC-10° and LLMC-10° are shown in Figure 12.

We can obtain an upper bound on ρ_{DDISC} for $|z| < 1.1\,\mathrm{kpc}$ from the kinematics of stars at the solar neighbourhood. Holmberg & Flynn (2000) find a local dynamical mass density of $0.102 \pm 0.01\mathrm{M}_\odot\,\mathrm{pc}^{-3}$ with $0.095\,\mathrm{M}_\odot\,\mathrm{pc}^{-3}$ in visible disc matter. This leaves room for a maximal dark density of $0.008\,\mathrm{M}_\odot\,\mathrm{pc}^{-3}$ which seems consistent with a dark halo and no dynamically significant dark disc. However, Statler (1989) have argued that model degeneracies in this analysis could lead to systematic errors as large as 30%. If we take this more generous limit, we can have a maximal density of $0.038\,\mathrm{M}_\odot\,\mathrm{pc}^{-3}$, which leaves room for a dynamically significant dark disc up to $\rho_{\mathrm{DDISC}}(R_\odot) = 3\rho_{\mathrm{HALO}}$. These limits will improve dramatically with the improved data from large kinematic surveys like RAVE and GAIA.

Interestingly, Kalberla (2003) and Kalberla et al. (2007) have recently argued for a dark disc in the Milky Way to explain the observed flaring in the HI gas. The dark disc they require has a scale height and length of $z_{1/2} = 2.8\,\mathrm{kpc}$, $R_{1/2} = 12.6\,\mathrm{kpc}$ and total mass $\sim 2 \times 10^{11}\,\mathrm{M}_\odot$. For LLMC-10°, our dark disc has total mass 8.6×10^9 for $|z| < 1.1\,\mathrm{kpc}$ and $3 \times 10^{10}\,\mathrm{M}_\odot$ for $|z| < 5\,\mathrm{kpc}$. While the half mass scale length and height of our dark disc match well those of Kalberla et al. (2007), our disc appears under-massive by an order of magnitude.

Even if dynamically uninteresting, the dark disc has important implications for the direct detection of dark matter because it rotates much more slowly with respect to the Earth than the Milky Way halo. The solar neighbourhood distribution functions for the thin disc, thick disc, dark disc and dark halo in LMC-10° are shown in Figure 14; we plot results from the *Earth frame* so that the dark halo appears to rotate, while the discs are stationary. Notice that the dark disc has very similar kinematics to the stellar thick disc. If the thick disc of the Milky Way is mostly accreted rather than heated stars, then this is useful. It means that we can obtain a good measure of the kinematics of the dark disc from observations of the stellar thick disc at the solar neighbourhood.

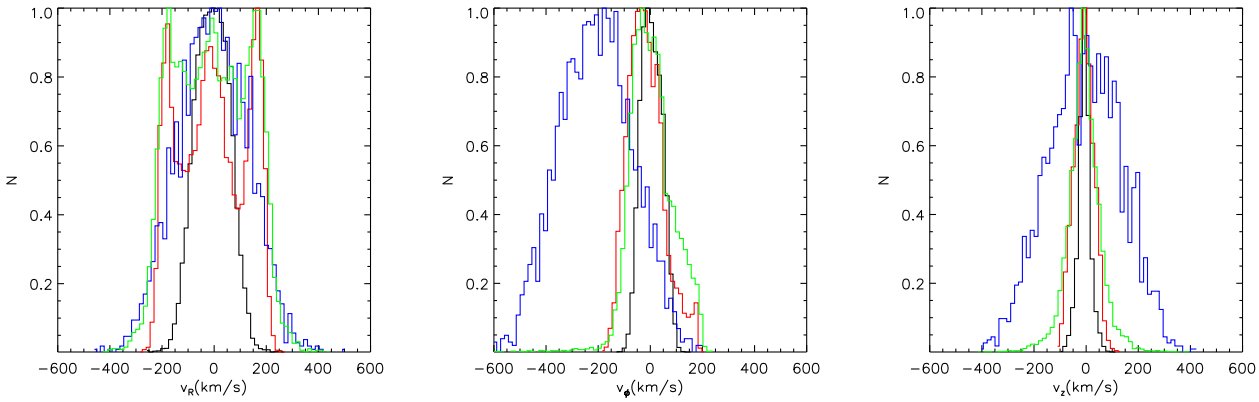

Figure 14. Distribution functions for the thin disc (black), thick disc (red), dark disc (green) and dark halo (blue) for LMC-10°at the solar neighbourhood ($8 < R < 9\,$kpc; $|z| < 0.35\,$kpc); we plot results from the *Earth frame* so that the dark halo appears to rotate, while the discs are stationary. The distributions are normalised to peak at 1 and do not represent the mass in each component. Notice that the dark disc has very similar kinematics to the stellar thick disc, except in that it has slightly larger σ_z. Similar results were found for our other runs. The radial velocity distribution is triple-peaked because the stars and dark matter are not fully phase mixed yet, even after 6.5 Gyrs.

The effect of the dark disc on the dark matter detection rate, the annual modulation signal, and on the dark matter capture rate by the Sun and Earth will be quantified in detail in forthcoming papers (Bruch, Lake, Read, Baudis in prep. 2008).

4 CONCLUSIONS

We have presented a detailed study of the effect of the Milky Way stellar disc on merging satellites in a ΛCDM cosmology. We have used both cosmological dark matter simulations of structure formation to assess the likelihood of near-disc plane accretion events, and collisionless simulations of satellite mergers to quantify the final state of the accreted material, and the effect on the Milky Way stellar disc. Our main findings are as follows:

(i) On average, a Milky Way-sized galaxy has 1.5 subhalos with peak circular speed $v_{\rm max} > 80\,$km/s; 5 with $v_{\rm max} > 60\,$km/s; and 13 with $v_{\rm max} > 40\,$km/s merge at redshift $z \gtrsim 1$. A third of these merge at an impact angle $\theta < 20^{\rm o}$ and are dragged into the disc plane by dynamical friction.

(ii) For an impact angle of $10^{\rm o} < \theta < 20^{\rm o}$, an eccentricity of $0.36 < e < 0.8$, and $v_{\rm max} = 60 - 80\,$km/s, the accreted material has almost all of the observational properties of the Galactic thick disc at the solar neighbourhood ($8 < R < 9\,$kpc), but the resultant accreted thick disc is under-massive by a factor $\sim 2 - 10$.

(iii) The most massive mergers at high redshift – $v_{\rm max} \gtrsim 80\,$km/s – heat the thin disc enough to produce a heated thick disc; none of the lower mass mergers provide enough heating. The heated thick disc is essential for obtaining a thick disc as massive as that observed in the Milky Way and likely contributes $\sim 50 - 90\%$ of the thick disc stars at the solar neighbourhood.

(iv) A key new point we make is that low inclination mergers – that must occur in a ΛCDM cosmology – also give rise to a thick disc of *dark matter*. The dark disc is of longer scale length and height than the accreted stellar thick disc ($R_{1/2} \sim 12\,$kpc, $z_{1/2} \sim 1.5\,$kpc), and provides $\sim 0.2 - 1$ times the density of the dark halo within $|z| < 1.1\,$kpc at the solar neighbourhood. The precise number depends on the satellite properties and the number of mergers. At all but the highest of these densities, the dark disc is not likely to be dynamically interesting. However, the dark disc does have important implications for the direct detection of dark matter because of its low velocity with respect to the Earth. A full quantitative analysis will be presented in a forthcoming paper (Bruch, Lake, Read, Baudis in prep. 2008).

(v) Higher inclination encounters $\theta > 20^{\rm o}$ are twice as likely as low inclination ones. These lead to structures that are hotter ($\sigma_z > 100\,$km/s), rotate more slowly ($v_c < 100\,$km/s), extend 10-20 kpc above the disc, and closely resemble the inner/outer stellar halos recently discovered by Carollo et al. (2007). The integrated light from such encounters is of order the total mass in the Milky Way stellar halo.

(vi) We quantify the effect these mergers have on the Milky Way disc. All encounters excite a bar, flare and warp in the disc that are long-lived. The bar is a poor indicator of merger activity because a bar formed by secular evolution (due to a more massive stellar disc) is longer and provides a better fit to the Milky Way bar than those induced by mergers. By contrast, the flare and warp are strong indicators of merger activity. Their strength grows with satellite impact angle and is not strongly affected by any other parameter – particularly at large radii ($R > 10\,$kpc). Of the simulations that we consider, a $v_{\rm max} = 60\,$km/s merger at $\theta = 60^{\rm o}$ to the Milky Way disc plane provides the best match to the observed Milky Way warp and flare.

(vii) Finally, we show that even $v_{\rm max} = 70\,$km/s galaxies have dynamical friction times longer than the age of the Universe once mass loss due to tides is taken into account. In practice, they merge much faster than this because they 'ride in' inside loosely bound groups that are ten times more massive. This should be taken into account when calculating the

orbits of Local Group satellite galaxies such as the Large and Small Magellanic Clouds, and the Sagittarius dwarf galaxy.

5 ACKNOWLEDGEMENTS

We would like to thank Joachim Stadel for providing the latest version of SKID and for very useful discussions. Thanks go to Doug Potter for making the zBox2 – the computer on which almost all the simulations presented here were run – fly. One simulation used the Arctic Region Supercomputer Center, for which we are grateful. Finally, we would like to thank Juerg Diemand for making his simulation output available to us.

REFERENCES

Abadi M. G., Navarro J. F., Steinmetz M., Eke V. R., 2003, ApJ, 597, 21
Agertz O., Moore B., Stadel J., Potter D., Miniati F., Read J., Mayer L., Gawryszczak A., Kravtsov A., Monaghan J., Nordlund A., Pearce F., Quilis V., Rudd D., six other authors. 2006, ArXiv Astrophysics e-prints
Ardi E., Tsuchiya T., Burkert A., 2003, ApJ, 596, 204
Azzaro M., Zentner A. R., Prada F., Klypin A. A., 2006, ApJ, 645, 228
Bailin J., 2003, ApJ, 583, L79
Bailin J., Power C., Norberg P., Zaritsky D., Gibson B. K., 2007, ArXiv e-prints, 706
Bailin J., Steinmetz M., 2005, in Jerjen H., Binggeli B., eds, IAU Colloq. 198: Near-fields cosmology with dwarf elliptical galaxies Can satellite dwarfs excite galactic warps?. pp 207–210
Bania T. M., Lockman F. J., 1984, ApJS, 54, 513
Belokurov V., Zucker D. B., Evans N. W., Gilmore G., Vidrih S., Bramich D. M., Newberg H. J., Wyse R. F. G., Irwin M. J., Fellhauer M., Hewett P. C., Walton N. A., Wilkinson M. I., 8 other authors 2006, ApJ, 642, L137
Bensby T., Zenn A. R., Oey M. S., Feltzing S., 2007, ApJ, 663, L13
Benson A. J., Lacey C. G., Frenk C. S., Baugh C. M., Cole S., 2004, MNRAS, 351, 1215
Bertschinger E., 2001, ApJS, 137, 1
Binney J., 2007, Dynamics of Disks. ISLAND UNIVERSES, Astrophysics and Space Science Proceedings. ISBN 978-1-4020-5572-0. Springer, 2007, p. 67, pp 67–+
Binney J., Jiang I.-G., Dutta S., 1998, MNRAS, 297, 1237
Binney J., Tremaine S., 2008, Galactic dynamics. Princeton, NJ, Princeton University Press, 2008, 747 p.
Bissantz N., Gerhard O., 2002, MNRAS, 330, 591
Brainerd T. G., 2005, ApJ, 628, L101
Brook C., Richard S., Kawata D., Martel H., Gibson B. K., 2007, ApJ, 658, 60
Brook C. B., Gibson B. K., Martel H., Kawata D., 2005, ApJ, 630, 298
Brook C. B., Kawata D., Gibson B. K., Freeman K. C., 2004, ApJ, 612, 894
Bullock J. S., Johnston K. V., 2005, ApJ, 635, 931
Burstein D., 1979, ApJ, 234, 829
Cabrera-Lavers A., Bilir S., Ak S., Yaz E., López-Corredoira M., 2007, A&A, 464, 565
Carollo D., Beers T. C., Lee Y. S., Chiba M., Norris J. E., Wilhelm R., Sivarani T., Marsteller B., Munn J. A., Bailer-Jones C. A. L., Re Fiorentin P., York D. G., 2007, ArXiv e-prints, 706
Ceverino D., Klypin A., 2007, ArXiv e-prints, 712
Conn B. C., Lane R. R., Lewis G. F., Gil-Merino R., Irwin M. J., Ibata R. A., Martin N. F., Bellazzini M., Sharp R., Tuntsov A. V., Ferguson A. M. N., 2007, MNRAS, 376, 939
Dalcanton J. J., Bernstein R. A., 2002, AJ, 124, 1328
Debattista V. P., Mayer L., Carollo C. M., Moore B., Wadsley J., Quinn T., 2006, ApJ, 645, 209
Debattista V. P., Sellwood J. A., 1999, ApJ, 513, L107
Dehnen W., Binney J., 1998, MNRAS, 294, 429
Diemand J., Madau P., Moore B., 2005, MNRAS, 364, 367
Diemand J., Moore B., Stadel J., 2004, MNRAS, 352, 535
D'Onghia E., 2008, ArXiv e-prints, 802
Dubinski J., Gauthier J.-R., Widrow L., Nickerson S., 2008, ArXiv e-prints, 802
Elmegreen B. G., Elmegreen D. M., 2006, ApJ, 650, 644
Faltenbacher A., Li C., Mao S., van den Bosch F. C., Yang X., Jing Y. P., Pasquali A., Mo H. J., 2007, ApJ, 662, L71
Font A. S., Navarro J. F., Stadel J., Quinn T., 2001, ApJ, 563, L1
Freeman K., Bland-Hawthorn J., 2002, ARA&A, 40, 487
Fulbright J. P., McWilliam A., Rich R. M., 2006, ApJ, 636, 821
Gao L., White S. D. M., Jenkins A., Stoehr F., Springel V., 2004, MNRAS, 355, 819
Gauthier J.-R., Dubinski J., Widrow L. M., 2006, ApJ, 653, 1180
Gerhard O., 2002, Space Science Reviews, 100, 129
Gilmore G., Reid N., 1983, MNRAS, 202, 1025
Gottlöber S., Klypin A., Kravtsov A. V., 2001, ApJ, 546, 223
Governato F., Willman B., Mayer L., Brooks A., Stinson G., Valenzuela O., Wadsley J., Quinn T., 2007, MNRAS, 374, 1479
Hayashi H., Chiba M., 2006, PASJ, 58, 835
Heitmann K., Lukic Z., Fasel P., Habib S., Warren M. S., White M., Ahrens J., Ankeny L., Armstrong R., O'Shea B., Ricker P. M., Springel V., Stadel J., Trac H., 2007, ArXiv e-prints, 706
Holmberg E., 1941, ApJ, 94, 385
Holmberg E., 1974, Arkiv for Astronomi, 5, 305
Holmberg J., Flynn C., 2000, MNRAS, 313, 209
Holmberg J., Flynn C., 2004, MNRAS, 352, 440
Huang S., Carlberg R. G., 1997, ApJ, 480, 503
Ibata R., Chapman S., Ferguson A. M. N., Lewis G., Irwin M., Tanvir N., 2005, ApJ, 634, 287
Ibata R., Martin N. F., Irwin M., Chapman S., Ferguson A. M. N., Lewis G. F., McConnachie A. W., 2007, ArXiv e-prints, 704
Ibata R. A., Gilmore G., Irwin M. J., 1994, Nature, 370, 194
Ibata R. A., Irwin M. J., Lewis G. F., Ferguson A. M. N., Tanvir N., 2003, MNRAS, 340, L21
Jurić M., Ivezić Ž., Brooks A., Lupton R. H., Schlegel D., Finkbeiner D., Padmanabhan N., Bond N., Sesar B., Rockosi C. M., Knapp G. R., Gunn J. E., Sumi T., Schnei-

der D. P., and 12 other authors. 2008, ApJ, 673, 864
Just A., Jahreiss H., 2007, ArXiv e-prints, 706
Kalberla P. M. W., 2003, ApJ, 588, 805
Kalberla P. M. W., Dedes L., Kerp J., Haud U., 2007, A&A, 469, 511
Kampczyk P., Lilly S. J., Carollo C. M., Scarlata C., Feldmann R., Koekemoer A., Leauthaud A., Taniguchi Y., Capak P., 2006, ArXiv Astrophysics e-prints
Karaali S., Bilir S., Hamzaoğlu E., 2004, MNRAS, 355, 307
Kazantzidis S., Bullock J. S., Zentner A. R., Kravtsov A. V., Moustakas L. A., 2007, ArXiv e-prints, 708
Kazantzidis S., Magorrian J., Moore B., 2004, ApJ, 601, 37
Kerr F. J., Bowers P. F., Jackson P. D., Kerr M., 1986, A&AS, 66, 373
Klypin A., Zhao H., Somerville R. S., 2002, ApJ, 573, 597
Kuijken K., Gilmore G., 1989, MNRAS, 239, 651
Lake G., 1989, AJ, 98, 1554
Lake G., D'Onghia E., 2008, ArXiv e-prints, 802
Levine E. S., Blitz L., Heiles C., Weinberg M., 2006, ArXiv Astrophysics e-prints
Li Y.-S., Helmi A., 2007, ArXiv e-prints, 711
López-Corredoira M., Cabrera-Lavers A., Garzón F., Hammersley P. L., 2002, A&A, 394, 883
López-Corredoira M., Cabrera-Lavers A., Mahoney T. J., Hammersley P. L., Garzón F., González-Fernández C., 2007, AJ, 133, 154
Ludlow A. D., Navarro J. F., Springel V., Jenkins A., Frenk C. S., Helmi A., 2008, ArXiv e-prints, 801
Macciò A. V., Moore B., Stadel J., Diemand J., 2006, MNRAS, 366, 1529
Majewski S. R., Skrutskie M. F., Weinberg M. D., Ostheimer J. C., 2003, ApJ, 599, 1082
Malhotra S., 1995, ApJ, 448, 138
Martinez-Delgado D., Pohlen M., Gabany R. J., Majewski S. R., Penarrubia J., Palma C., 2008, ArXiv e-prints, 801
Matthews L. D., 2000, AJ, 120, 1764
Moore B., Ghigna S., Governato F., Lake G., Quinn T., Stadel J., Tozzi P., 1999, ApJ, 524, L19
Morrison H. L., 1993, AJ, 106, 578
Naab T., Ostriker J. P., 2006, MNRAS, 366, 899
Nelson R. W., Tremaine S., 1995, MNRAS, 275, 897
Nordström B., Mayor M., Andersen J., Holmberg J., Pont F., Jørgensen B. R., Olsen E. H., Udry S., Mowlavi N., 2004, A&A, 418, 989
Ojha D. K., 2001, MNRAS, 322, 426
Peñarrubia J., McConnachie A., Babul A., 2006, ApJ, 650, L33
Pohlen M., Balcells M., Lütticke R., Dettmar R.-J., 2004, A&A, 422, 465
Prochaska J. X., Naumov S. O., Carney B. W., McWilliam A., Wolfe A. M., 2000, AJ, 120, 2513
Quinn P. J., Goodman J., 1986, ApJ, 309, 472
Quinn P. J., Hernquist L., Fullagar D. P., 1993, ApJ, 403, 74
Read J. I., Wilkinson M. I., Evans N. W., Gilmore G., Kleyna J. T., 2006a, MNRAS, 367, 387
Read J. I., Wilkinson M. I., Evans N. W., Gilmore G., Kleyna J. T., 2006b, MNRAS, 366, 429
Ricotti M., Gnedin N. Y., Shull J. M., 2002, ApJ, 575, 33
Robertson B., Yoshida N., Springel V., Hernquist L., 2004, ApJ, 606, 32
Rocha-Pinto H. J., Scalo J., Maciel W. J., Flynn C., 2000, A&A, 358, 869
Sales L. V., Navarro J. F., Abadi M. G., Steinmetz M., 2007, ArXiv e-prints, 704
Sales L. V., Navarro J. F., Lambas D. G., White S. D. M., Croton D. J., 2007, ArXiv e-prints, 706
Seabroke G. M., Gilmore G., 2007, ArXiv e-prints, 707
Seljak U., Slosar A., McDonald P., 2006, Journal of Cosmology and Astro-Particle Physics, 10, 14
Sellwood J. A., Nelson R. W., Tremaine S., 1998, ApJ, 506, 590
Shen J., Sellwood J. A., 2006, MNRAS, 370, 2
Soubiran C., Bienaymé O., Siebert A., 2003, A&A, 398, 141
Spergel D. N., Bean R., Doré O., Nolta M. R., Bennett C. L., Dunkley J., Hinshaw G., Jarosik N., Komatsu E., Page L., Peiris H. V., Verde L., Halpern M., nine other authors 2007, ApJS, 170, 377
Stadel J. G., 2001, Ph.D. Thesis, Univ. Washington
Statler T. S., 1989, ApJ, 344, 217
Stewart K. R., Bullock J. S., Wechsler R. H., Maller A. H., Zentner A. R., 2007, ArXiv e-prints, 711
Thacker R. J., Couchman H. M. P., 2000, ApJ, 545, 728
Toomre A., Toomre J., 1972, ApJ, 178, 623
Tsikoudi V., 1977, PhD thesis, AA(Texas Univ., Austin.)
van der Marel R. P., Alves D. R., Hardy E., Suntzeff N. B., 2002, AJ, 124, 2639
van Dokkum P. G., Peletier R. F., de Grijs R., Balcells M., 1994, A&A, 286, 415
Velazquez H., White S. D. M., 1999, MNRAS, 304, 254
Villalobos A., Helmi A., 2008, arXiv:0803.2323 [astro-ph]
Vogelsberger M., White S. D. M., Helmi A., Springel V., 2008, MNRAS, pp 143–+
Walker I. R., Mihos J. C., Hernquist L., 1996, ApJ, 460, 121
Walker M. G., Mateo M., Olszewski E. W., Bernstein R., Wang X., Woodroofe M., 2006, AJ, 131, 2114
Weaver H., Williams D. R. W., 1973, A&AS, 8, 1
Weaver H., Williams D. R. W., 1974, A&AS, 17, 251
Wilkinson M. I., Evans N. W., 1999, MNRAS, 310, 645
Yoachim P., Dalcanton J. J., 2005, ApJ, 624, 701
Yoachim P., Dalcanton J. J., 2006, AJ, 131, 226
Younger J. D., Besla G., Cox T. J., Hernquist L., Robertson B., Willman B., 2008, ArXiv e-prints, 802
Zhao H., 2004, MNRAS, 351, 891